

**CHANGEPOINT PROBLEM WITH ANGULAR DATA  
USING A MEASURE OF VARIATION BASED ON  
THE INTRINSIC GEOMETRY OF TORUS**

Surojit Biswas

surojit23@iitkgp.ac.in

Department of Mathematics, Indian Institute of Technology Kharagpur, India-721302

and

Buddhananda Banerjee

bbanerjee@maths.iitkgp.ac.in

Department of Mathematics, Indian Institute of Technology Kharagpur, India-721302

and

Arnab Kumar Laha

arnab@iima.ac.in

Operations and Decision Sciences Area, Indian Institute of Management Ahmedabad,  
India-380015

ABSTRACT. In many temporally ordered data sets, it is observed that the parameters of the underlying distribution change abruptly at unknown times. The detection of such change-points is important for many applications. While this problem has been studied substantially in the linear data setup, not much work has been done for angular data. In this article, we utilize the intrinsic geometry of a torus to introduce the notion of the “square of an angle” and use it to propose a new measure of variation, called the “curved variance”, of an angular random variable. Using the above ideas, we propose new tests for the existence of changepoint(s) in the concentration, mean direction, and/or both of these. The limiting distributions of the test statistics are derived and their powers are obtained using extensive simulation. It is seen that the tests have better power than the corresponding existing tests. The proposed methods have been implemented on three real-life data sets revealing interesting insights. In particular, our method when used to detect simultaneous changes in mean direction and concentration for hourly wind direction measurements of the cyclonic storm “Amphan” identified changepoints that could be associated with important meteorological events.

Keywords: Angular data; Torus; First fundamental form ; Area element; Cumulative sum; changepoint.

---

<sup>0</sup>corresponding author: bbanerjee@maths.iitkgp.ernet.in

## CONTENTS

1. Introduction	3
2. Curved Variance	5
2.1. Intrinsic geometry of torus	6
2.2. Defining “curved variance” for circular data	6
3. Changepoint detection	10
3.1. Changepoint detection for concentration	10
3.2. Changepoint detection for mean direction	11
3.3. Changepoint detection- The general case	13
4. Numerical Studies	14
5. Data analysis	17
5.1. Circular Temporal Plot	17
5.2. Acrophase Data:	18
5.3. Flare Data:	18
5.4. Amphan Cyclone Data:	19
6. Conclusion	20
References	21
7. Appendix	22

## 1. INTRODUCTION

Angular data ( a.k.a. directional data or circular data) arises from the study of phenomena that are circular or periodic. In contrast to linear data, there is no universally accepted ordering of circular data for its entire range. The choice of the zero direction and the clockwise or anti-clockwise orientation play a critical role while working with circular data. Examples of circular data include angular measurements such as active galactic nuclei (astronomy), dihedral angles of protein structure (bio-informatics), wind direction (meteorology), sea wave direction (climatology), etc. The reader can refer to [Mardia \(2000\)](#) for a more in-depth exploration of circular data.

Changepoint analysis is an important statistical concept to detect unexpected shifts or alterations within a temporally ordered data set. These changes might be caused by a change in the parameter(s) within the same family of distributions or a complete change in the family of distributions. The usual statistical analysis of data gets heavily affected because of the existence of changepoints in the data set. Therefore, the primary goal of changepoint analysis is to conduct a statistical test to check for the existence of a changepoint in a given sequence of data. A substantial amount of research in changepoint analysis has been carried out for real-valued random variables (see [Fearnhead and Rigail, 2019](#); [Haynes et al., 2017](#); [Horváth et al., 1999](#); [Antoch et al., 1997](#); [Cobb, 1978](#); [Davis et al., 1995](#)), vector-valued random variable (see [Kirch et al., 2015](#); [Kokoszka and Leipus, 2000](#); [Shao and Zhang, 2010](#); [Anastasiou and Papanastasiou, 2023](#); [Pishchagina et al., 2023](#)), and functional valued random variable (see [Horváth and Kokoszka, 2012](#); [Banerjee and Mazumder, 2018](#); [Hörmann and Kokoszka, 2010](#); [Banerjee et al., 2020](#)). In the context of angular data, there has been limited exploration of the changepoint problem. The changepoint in angular data may occur in the mean direction, concentration, or both. For the first time, [Lombard \(1986\)](#) introduced a pioneering rank-based test to detect changepoints in the location change, and change in concentration parameter for angular data. Following this work, [Grabovsky and Horváth \(2001\)](#) put forth a modified CUSUM procedure for testing the change in concentration parameter of the angular distribution. [Ghosh et al. \(1999\)](#), proposed a likelihood-based approach for addressing changepoint detection in the mean direction for the von Mises distribution only. Additionally, [SenGupta and Laha \(2008\)](#) introduced a novel likelihood-based method, referred to as the likelihood integrated method. These collective efforts mark significant strides in developing methodologies to discern changepoints within the domain of angular data.

In this article, we deal with the changepoint problems of angular data in concentration, mean direction, and/or both. We introduce a new notion of the ‘square of an angle’ with the help of the intrinsic geometry of a curved torus to develop a measure analogous to the variance

of linear data which we call ‘curved variance’. Employing this concept of the ‘square of an angle’, we propose a test for identifying the changepoint(s) in the concentration of angular data. We also obtain the asymptotic pivotal distribution of the test statistic under the null hypothesis of no change, which is free from the concentration as well as the mean direction (which is a nuisance parameter). We will refer to this test as the *Square Angle Concentration Change (SACC)* test in the rest of the paper. An extensive simulation study shows that the SACC test is more powerful compared to the existing one by [Grabovsky and Horváth \(2001\)](#). Furthermore, using the notion of ‘curved variance’ we have also constructed a test for identifying the presence of changepoint(s) in the mean direction, which in simulation studies perform equally well with the maximum likelihood ratio test proposed by [Ghosh et al. \(1999\)](#) for the data from von Mises distribution. We will refer to this test as the *Curved Variance Mean Change (CVMC)* test in the rest of the paper. This proposed test is extendable in a straightforward manner to other circular distributions, which is not the case for the test given by [Ghosh et al. \(1999\)](#) because of challenges in the computation of the maximum likelihood estimates of parameters for circular distributions. Again, using the notion of ‘square of an angle’ we propose a new test for detecting changepoint(s) for the mean direction and/or the concentration in general. We will refer to this test as the *Square Angle General Change (SAGC)* test in the rest of the paper.

We illustrate the method for detecting changepoints in concentration on the Acrophase data set (see [Lombard et al., 2017](#)) related to systolic blood pressure (SBP) in a patient undergoing clinical depression episodes. The results reveal that the proposed methods effectively identify changepoints in concentration. The method for detecting changepoints in the mean direction has been implemented on the Flare data set (see [Lombard, 1986](#)). Lastly, we have executed the method for detecting changepoints in the concentration and/or mean direction on a weather data set (see [Hersbach et al., 2023](#)) of a super cyclonic storm “Amphan” over the Bay of Bengal that severely hit and caused extensive damages in eastern India and Bangladesh during the period 16th May 2020 to 21st May 2020. A newly developed exploratory graphical data analysis tool *Circular temporal plot* (see Section 5.1 for a description of the plot) is used to guide the presence of changepoints in a temporally ordered data set of angular observations.

Let  $\theta_1, \theta_2, \dots, \theta_n \in [0, 2\pi)$  be angular random variables. A changepoint is defined as a fixed and unknown point  $k^* \in \{0, 1, \dots, n\}$  such that  $\theta_1, \theta_2, \dots, \theta_{k^*}$  follow a distribution  $F(\theta; \lambda_1)$ , and  $\theta_{k^*+1}, \theta_{k^*+2}, \dots, \theta_n$  follow a different distribution  $F(\theta; \lambda_2)$ , where  $\lambda_1 \neq \lambda_2$ , and  $F(\theta; \lambda_1) \neq F(\theta; \lambda_2)$  for all  $\theta \in [0, 2\pi)$ . The flow of the work is given below. After studying the intrinsic geometry of the curved torus in Section 2.1 we introduce the definition of *Curved Variance* for circular data. Section 3 is dedicated to changepoint detection in

concentration with known mean direction (Section 3.1), changepoint detection in mean direction with known concentration value (Section 3.2), and changepoint detection in either of the parameters (Section 3.3) when both are unknown. Section 4 presents a comparison of the proposed method with existing methods for different circular distributions namely, von Mises, Kato-Jones, and Wrapped Cauchy. In Section 5, we implement the proposed methods for changepoint detection in concentration for Acrophase data (Section 5.2), in mean direction for Flare data (Section 5.3), and in both for Amphan super cyclone data (Section 5.4). The concluding Section 6 is followed by the algorithms related to the proposed tests provided in Section-7.

## 2. CURVED VARIANCE

Before getting into the proposed methods, we briefly discuss some basic tools from Riemannian geometry. Here, we introduce a few definitions of tangent space, the first fundamental form, and the area element. The reader may see Gallier and Quaintance (2020) for details.

**Definition 1.** Let  $\mathcal{M}$  be a Riemannian surface. Then the set of all tangent vectors  $v$  at  $x \in \mathcal{M}$  is called the **tangent space** to the point  $x$  and it is denoted by  $T_x\mathcal{M}$ .

Let  $\mathcal{M} \subset \mathbb{R}^3$  be a Riemannian surface defined by  $X : \mathbb{R}^2 \rightarrow \mathcal{M}$ . Then a curve  $\gamma(t)$  on  $\mathcal{M}$  parametrized by  $t \in [a, b]$  can be defined as  $\gamma(t) = X(u(t), v(t))$ . Therefore, the velocity vector can be obtained as

$$\gamma'(t) = \frac{\partial X}{\partial u} \frac{du}{dt} + \frac{\partial X}{\partial v} \frac{dv}{dt} = [X_u, X_v][u', v']^T$$

Thus, we can represent the velocity vector as the linear combination of the basis vectors  $X_u = \frac{\partial X}{\partial u}$  and  $X_v = \frac{\partial X}{\partial v}$ , with coefficients  $u' = \frac{du}{dt}$  and  $v' = \frac{dv}{dt}$ . Let  $s(t)$  be the arc length along  $\gamma$  with  $s(a) = 0$  then  $s(t) = \int_a^t \|\gamma'(r)\| dr$ , so, we have  $\frac{ds}{dt} = \|\gamma'(t)\|$ . Now, the **first fundamental form** or **metric form** of the surface  $\mathcal{M}$  can be obtained as

$$\begin{aligned} \left(\frac{ds}{dt}\right)^2 &= \langle \gamma'(t), \gamma'(t) \rangle \\ &= \langle (u'X_u + v'X_v), (u'X_u + v'X_v) \rangle \\ &= (u')^2 \langle X_u, X_u \rangle + 2u'v' \langle X_u, X_v \rangle + (v')^2 \langle X_v, X_v \rangle \\ &\equiv (u')^2 E + 2u'v' F + (v')^2 G \\ &= \begin{bmatrix} u' \\ v' \end{bmatrix}^T \begin{bmatrix} E & F \\ F & G \end{bmatrix} \begin{bmatrix} u' \\ v' \end{bmatrix} \end{aligned}$$

where  $E = \langle X_u, X_u \rangle$ ,  $F = \langle X_u, X_v \rangle$ , and  $G = \langle X_v, X_v \rangle$ , with usual inner-product  $\langle \cdot, \cdot \rangle$ .

**Definition 2.** The area element,  $dA$  of the surface  $\mathcal{M}$  determined by  $X(u, v)$  is defined by

$$dA = |X_u \times X_v| \, dudv = \sqrt{EG - F^2} \, dudv.$$

Hence, the total surface area of the surface  $\mathcal{M}$  is

$$A = \int \int dA \, dudv = \int \int \sqrt{EG - F^2} \, dudv.$$

**2.1. Intrinsic geometry of torus.** The rest of our work will be based on the curved torus defined by the parametric equation

$$X(\phi, \theta) = \{(R + r \cos \theta) \cos \phi, (R + r \cos \theta) \sin \phi, r \sin \theta\} \subset \mathbb{R}^3, \quad (1)$$

with the parameter space  $\{(\phi, \theta) : 0 < \phi, \theta < 2\pi\} = \mathbb{S}_1 \times \mathbb{S}_1$ , known as flat torus. Now, the partial derivatives of  $X$  with respect to  $\phi$ , and  $\theta$  are

$$X_\phi = \{-(R + r \cos \theta) \sin \phi, (R + r \cos \theta) \cos \phi, 0\}$$

and

$$X_\theta = \{-r \sin \theta \cos \phi, -r \sin \theta \sin \phi, r \cos \theta\}$$

respectively. Hence, the coefficients of the first fundamental form are

$$\begin{aligned} E &= \langle X_\phi, X_\phi \rangle = (R + r \cos \theta)^2 \\ F &= \langle X_\phi, X_\theta \rangle = 0 \\ G &= \langle X_\theta, X_\theta \rangle = r^2 \end{aligned} \quad (2)$$

leading to the area element of the curved torus (Equation-1)

$$dA = r(R + r \cos \theta) \, d\phi \, d\theta \quad (3)$$

from the Definition-2. We will use this idea to introduce the notion of curved variance, a new notion of variation for angular random variables.

**2.2. Defining “curved variance” for circular data.** Before introducing the notion of Curved Variance (CVar), we begin by taking a fresh look at the usual idea of variance for a univariate linear random variable. Let  $X$  be a univariate random variable on  $\mathbb{R}$  with a probability density function  $f(x)$ , and  $E(X) = \mu$ , then the variance of  $X$  can be expressed as

$$\text{Var}(X) = E(X - \mu)^2 = E(Z^2). \quad (4)$$

where  $Z = (X - \mu)$ . Observe that  $Z^2$  can be viewed as the area of a square with side  $Z$ , enclosed by the lines  $x = 0$ ,  $y = 0$ ,  $x = Z$ , and  $y = Z$ . Thus, the variance of  $X$  can be

interpreted as the expectation of the area of a random square with side  $Z$ . For multivariate random vector  $\mathbf{X}$  with mean vector  $\boldsymbol{\mu}$ , the notion of variance is extended to generalized variance, which is the determinant of the dispersion matrix

$$D(\mathbf{X}) = E[(\mathbf{X} - \boldsymbol{\mu})(\mathbf{X} - \boldsymbol{\mu})^T] = E\mathbf{X}\mathbf{X}^T - \boldsymbol{\mu}\boldsymbol{\mu}^T.$$

Note that, determinant of  $D(\mathbf{X})$  is the volume of the parallelepiped with sides given by the eigenvalues of  $D(\mathbf{X})$ . Motivated by the above, we define the curved variance (Cvar) of a circular random variable as an area on the torus, the details of which are given below.

Let  $\phi, \theta \in [0, 2\pi)$  denote the horizontal and vertical angles of a torus, respectively. We begin by defining the area between two points on the surface of the torus. Let  $(\phi_1, \theta_1)$  and  $(\phi_2, \theta_2)$  be two points on the flat torus  $[0, 2\pi) \times [0, 2\pi)$ , then the *proportionate area included between these two diagonally opposite points* when mapped on the surface of the torus with horizontal and vertical radius  $R$  and  $r$ , respectively can be computed by using Equation-3 considering  $0 < \phi_1 < \phi_2 < 2\pi$  and  $0 < \theta_1 < \theta_2 < 2\pi$ . Note that for two such diagonally opposite points  $(\phi_1, \theta_1)$  and  $(\phi_2, \theta_2)$  on flat torus, the surface on the curve torus get partitioned into four mutually exclusive and exhaustive subsets as images (using Equation-1) of the following sets  $\mathbb{T}_1 := [\phi_1, \phi_2] \times [\theta_1, \theta_2]$ ,  $\mathbb{T}_2 := ([\phi_2, 2\pi] \cup [0, \phi_1]) \times [\theta_1, \theta_2]$ ,  $\mathbb{T}_3 := [\phi_1, \phi_2] \times ([\theta_2, 2\pi] \cup [0, \theta_1])$  and  $\mathbb{T}_4 := ([\phi_2, 2\pi] \cup [0, \phi_1]) \times ([\theta_2, 2\pi] \cup [0, \theta_1])$  with the corresponding areas  $A_1, A_2, A_3$  and  $A_4$  respectively. A diagrammatic representation of this decomposition is given in Figure-1. We now provide details of the computation of the areas  $A_1, A_2, A_3$  and  $A_4$  below.

- Case-1: Using Equation-3 on  $\mathbb{T}_1$  we get

$$\begin{aligned} A_1 &= \iint_{\mathbb{T}_1} dA = \int_{\phi_1}^{\phi_2} \int_{\theta_1}^{\theta_2} dA \\ &= rR \int_{\phi_1}^{\phi_2} d\phi \int_{\theta_1}^{\theta_2} \left(1 + \frac{r}{R} \cos \theta\right) d\theta. \\ &= rR(\phi_2 - \phi_1) \left[ (\theta_2 - \theta_1) + \frac{r}{R} (\sin \theta_2 - \sin \theta_1) \right]. \end{aligned} \quad (5)$$

- Case-2: Using Equation-3 on  $\mathbb{T}_2$  we get

$$\begin{aligned} A_2 &= \iint_{\mathbb{T}_2} dA = \int_{\phi_2}^{2\pi} \int_{\theta_1}^{\theta_2} dA + \int_0^{\phi_1} \int_{\theta_1}^{\theta_2} dA \\ &= rR[2\pi - (\phi_2 - \phi_1)] \left[ (\theta_2 - \theta_1) + \frac{r}{R} (\sin \theta_2 - \sin \theta_1) \right] \end{aligned} \quad (6)$$

- Case-3: Using Equation-3 on  $\mathbb{T}_3$  we get

$$A_3 = \iint_{\mathbb{T}_3} dA = \int_{\phi_1}^{\phi_2} \int_{\theta_2}^{2\pi} dA + \int_{\phi_1}^{\phi_2} \int_0^{\theta_1} dA$$

$$= rR(\phi_2 - \phi_1) \left[ (2\pi - (\theta_1 - \theta_2)) + \frac{r}{R}(\sin \theta_1 - \sin \theta_2) \right] \quad (7)$$

- Case-4: Using Equation-3 on  $\mathbb{T}_4$  we get

$$\begin{aligned} A_4 &= \iint_{\mathbb{T}_4} dA = \int_{\phi_2}^{2\pi} \int_{\theta_2}^{2\pi} dA \\ &+ \int_{\phi_2}^{2\pi} \int_0^{\theta_1} dA + \int_0^{\phi_1} \int_{\theta_2}^{2\pi} dA + \int_0^{\phi_1} \int_0^{\theta_1} dA \\ &= rR [2\pi - (\phi_2 - \phi_1)] \left[ (2\pi - (\theta_1 - \theta_2)) + \frac{r}{R}(\sin \theta_1 - \sin \theta_2) \right]. \end{aligned} \quad (8)$$

Analogous to the notion of circular distance - which is the length of the smaller arc between two angles, and the notion of geodesic distance on a surface - which is the length of the shortest path joining two points on the surface, we define the *proportionate area included between these two diagonally opposite points*  $(\phi_1, \theta_1)$ ,  $(\phi_2, \theta_2)$  as given Definition-3 below. It may be noted that, since  $r$  and  $R$  are arbitrary and  $\min\{A_1, A_2, A_3, A_4\}$  is dependent on  $rR$ , we divide it by  $4\pi^2 rR$  which is the total area of the torus to make it free from the product  $rR$ .

**Definition 3.** The *proportionate area included between the two diagonally opposite points*  $(\phi_1, \theta_1)$ ,  $(\phi_2, \theta_2)$  is defined as

$$A_T [(\phi_1, \theta_1), (\phi_2, \theta_2)] = \frac{\min\{A_1, A_2, A_3, A_4\}}{4\pi^2 rR}.$$

Following the above Definition-3, we obtain the proportionate area from  $(0, 0)$  to any arbitrary point  $(\phi, \theta)$  as:

$$A_T^{(0)}(\phi, \theta) = A_T [(0, 0), (\phi, \theta)]. \quad (9)$$

Now we apply this notion to circular random variables to define the square of an angle, which will be useful for defining the curved variance given in Definition-5 below.

**Definition 4.** The *square of an angle*  $\theta$  is defined as

$$A_C^{(0)}(\theta) = A_T^{(0)}(\theta, \theta) = A_T [(0, 0), (\theta, \theta)], \text{ where } \frac{r}{R} = 1. \quad (10)$$

**Definition 5.** Let  $\Theta$  be a zero-centered circular random variable with probability density function  $f(\theta)$  on the unit circle  $\mathbb{S}_1$ . Then, the *curved variance* of the random variable  $\Theta$  is

$$CVar(\Theta) = E_f \left[ A_C^{(0)}(\Theta) \right].$$

If the circular mean of  $\Theta$  is  $\mu \neq 0$  then  $\Theta$  can be replaced by  $\Theta' = [(\Theta - \mu) \bmod 2\pi]$ .



If a random sample  $\theta_1, \dots, \theta_n$  is given then using WLLN,  $CVar(\Theta)$  can be consistently estimated as  $\widehat{CVar}(\Theta) = \frac{1}{n} \sum_{i=1}^n A_C^{(0)} [(\theta_i - \mu) \bmod 2\pi]$ , when  $\mu$  is known.

When  $\mu$  is unknown we can use the plug-in estimator  $\widehat{CVar}(\Theta) = \frac{1}{n} \sum_{i=1}^n A_C^{(0)} [(\theta_i - \hat{\mu}) \bmod 2\pi]$ , where  $\hat{\mu}$  is the estimated circular mean of the data. From the above discussion, we have the following observations

**Remark 1.** The proportionate area  $A_T [(\phi_1, \theta_1)(\phi_2, \theta_2)] \in [0, \frac{1}{4}]$ . It may be noted that  $A_T [(\phi_1, \theta_1)(\phi_2, \theta_2)]$  only depends only on  $\frac{r}{R}$  where,  $0 < \frac{r}{R} \leq 1$ .

**Remark 2.**  $CVar$  does not depend on the (known) mean direction.

**Remark 3.** As a natural choice, put  $(\phi, \theta) = (0, 0)$  in Equation-1, the zero-point on the curved torus is assumed to be  $(R + r, 0, 0)$ , and counter-clock-wise rotation is considered to be conventional.

**Remark 4.** For univariate linear random variable  $X$  with expectation  $\eta$  it is well-known that

$$Var(X) = E(X - \eta)^2 = EX^2 - \eta^2.$$

Though Definition-5 is a generalization of the definition  $Var(X) = E(X - \eta)^2$ , but the simplification  $Var(X) = EX^2 - \eta^2$  is not generalizable to the case of angular data. i.e.  $E_f(A_C^{(0)} [(\Theta - \mu) \bmod 2\pi]) \neq E_f(A_C^{(0)}(\Theta)) - A_C^{(0)}(\mu)$  in general, where  $\Theta$  is a circular random variable with circular mean  $\mu$ . Consider a circular random variable  $\Theta$  with probability density function  $f(\theta)$  and mean direction at  $\pi$  as a counter-example. Note that

$$A_C^{(0)}(\theta) - A_C^{(0)}(\pi) = A_C^{(0)}(\theta) - \frac{1}{4} \leq 0 \text{ for all } \theta \in [0, 2\pi).$$

As a consequence  $E_f \left[ A_C^{(0)}(\Theta) \right] - \frac{1}{4} \leq 0$ . Hence,  $E_f \left[ A_C^{(0)}(\Theta) \right] - \frac{1}{4} < 0$  unless  $\Theta$  is degenerate at  $\pi$ . Thus we see that  $CVar(\Theta) = E_f(A_C^{(0)} [(\Theta - \pi) \bmod 2\pi]) \neq E_f(A_C^{(0)}(\Theta)) - A_C^{(0)}(\pi)$  when  $\Theta$  is not degenerate at  $\pi$ .

**Remark 5.** The definition of  $CVar$  considers the non-constant curvature through the area element of the surface of the torus. A similar approach, when applied to linear univariate data, would yield the usual definition of variance of linear univariate data since the curvature is constant.

The CUSUM technique (see [Grabovsky and Horváth, 2001](#)) is used to construct the test statistic identifying the changepoint in the concentration, whereas a likelihood ratio (see [Ghosh et al., 1999](#)) has been used to detect the changepoint in the mean direction. Using

the concept of ‘square of an angle’ we now propose a test statistic to test the existence of a changepoint in the concentration,  $[E^2(\cos \Theta) + E^2(\sin \Theta)]^{1/2}$ , and using the ‘curved variance’ we introduced a test for the mean direction  $\left[ \tan^{-1*} \left( \frac{E(\sin \Theta)}{E(\cos \Theta)} \right) \right]$ . A similar idea has been extended to construct a test in concentration and/or mean direction in a sequence of angular data. Where  $\tan^{-1*}$  is the quadrant specific inverse of the tangent (see [Jammalamadaka and Sengupta, 2001](#), p13, Equation-1.3.5).

### 3. CHANGEPOINT DETECTION

**3.1. Changepoint detection for concentration.** Let  $\theta_1, \theta_2, \dots, \theta_n \in [0, 2\pi)$  be independent angular random variables. We consider the following testing problem :

$$\begin{aligned} H_{0c} &: \theta_i \stackrel{\text{i.i.d.}}{\sim} F(\theta; \kappa_1) \text{ for all } i = 1, 2, \dots, n, \\ H_{1c} &: \begin{cases} \theta_i \stackrel{\text{i.i.d.}}{\sim} F(\theta; \kappa_1) & , 1 \leq i \leq k^* \\ \theta_i \stackrel{\text{i.i.d.}}{\sim} F(\theta; \kappa_2) & , (k^* + 1) \leq i \leq n, \end{cases} \end{aligned} \quad (11)$$

where  $F$  is a circular distribution with known mean direction  $\mu$ , common for all  $\theta_i$ , and concentration  $\kappa_1 \neq \kappa_2$  under  $H_{1c}$ .

Let  $a_i = A_C^{(0)}[(\theta_i - \mu) \bmod 2\pi]$  for  $i = 1, 2, \dots, n$ . Note that,  $a_i$ 's are i.i.d real valued random variables under the null hypothesis,  $H_{0c}$  with variance

$$\sigma_a^2 = \text{Var}(a_1) \hat{=} \frac{1}{n-1} \sum_{i=1}^n (a_i - \bar{a})^2 = \hat{\sigma}_a^2,$$

where  $n\bar{a} = \sum_{i=1}^n a_i$ . Now, we define a CUSUM process as

$$T(k) = \frac{1}{n \hat{\sigma}_a^2} \left[ \sum_{i=1}^k a_i - k\bar{a} \right]^2 \text{ for all } k = 1, \dots, n \quad (12)$$

to construct the test statistic

$$\Lambda_n = \max_{1 \leq k < n} \frac{T(k)}{\sqrt{\frac{k}{n} \left(1 - \frac{k}{n}\right)}}. \quad (13)$$

Here, we reject the null hypothesis,  $H_{0c}$ , if  $\Lambda_n > l_\alpha$ , where,  $l_\alpha$  is the upper  $\alpha$  point of the exact (or asymptotic) distribution of  $\Lambda_n$ . The closed-form distribution of  $\Lambda_n$  is not available, hence, we need to take recourse to simulation to obtain the cut-off value  $l_\alpha$ . But, when  $n$  is large, the limiting distribution of  $\Lambda_n$  can be derived as follows.

Let us consider  $u \in (0, 1)$ , and denote  $k = \lfloor nu \rfloor$ . Hence, from Equation-12 we can write

$$T_n(u) = T(\lfloor nu \rfloor) = \left( \frac{1}{\sqrt{n} \hat{\sigma}_a} \left[ \sum_{i=1}^{\lfloor nu \rfloor} a_i - u \sum_{i=1}^n a_i \right] \right)^2. \quad (14)$$

Then with the proper embedding of Skorohod topology in  $D[0, 1]$  (see Billingsley, 2013, Ch. 3), under the null hypothesis,  $H_{0c}$ , and as  $n \uparrow \infty$ , the process  $T_n(u)$  converges weakly to  $B_0^2(u)$ , where  $B_0(u)$  is the standard Brownian bridge on  $[0, 1]$ . As a consequence

$$\Lambda_n \xrightarrow{d} \sup_{0 < u < 1} B_0^2(u) = B_\infty, \text{ say.} \quad (15)$$

Hence, we can compute the upper- $\alpha$  value,  $l_\alpha$ , from the above limiting distribution of the test statistic (Equation-15). When the common mean direction ( $\mu$ ) of the data is unknown, it can be estimated by the circular mean ( $\hat{\mu}$ ) of the entire sample, and the  $a_i$ 's in Equation-12 can be replaced by

$$\hat{a}_i = A_C^{(0)}[(\theta_i - \hat{\mu}) \bmod 2\pi] \text{ for } i = 1, 2, \dots, n$$

to define  $\hat{T}(k)$  which will provide a test statistic similar to  $\Lambda_n$ , namely,

$$\hat{\Lambda}_n = \max_{1 \leq k < n} \frac{\hat{T}(k)}{\sqrt{\frac{k}{n} \left(1 - \frac{k}{n}\right)}}. \quad (16)$$

From Figure-2(A), it can be seen that the large sample distribution of the test statistic  $\Lambda_n$  under the null hypothesis,  $H_{0c}$ , is close to the distribution of  $B_\infty$ . Also note that when the common mean direction is unknown, the large sample distribution (see, Figure-2(B)) of the test statistic  $\hat{\Lambda}_n$  is well approximated by that of the  $B_\infty$ . under  $H_{0c}$ . Hence, the cut-off value obtained from the distribution  $B_\infty$  can be used to conduct an upper-tail test. Thus, for the SAAC test we

$$\text{Reject } H_{0c} \text{ if } l_\alpha < \hat{\Lambda}_n. \quad (17)$$

at level  $\alpha$ .

**3.2. Changepoint detection for mean direction.** Let  $\theta_1, \theta_2, \dots, \theta_n \in [0, 2\pi)$  be independent angular random variables. We consider the following testing problem:

$$\begin{aligned} H_{0m} &: \theta_i \stackrel{\text{i.i.d.}}{\sim} F(\theta; \mu_1) \text{ for all } i = 1, 2, \dots, n, \\ H_{1m} &: \begin{cases} \theta_i \stackrel{\text{i.i.d.}}{\sim} F(\theta; \mu_1) & , 1 \leq i \leq k^* \\ \theta_i \stackrel{\text{i.i.d.}}{\sim} F(\theta; \mu_2) & , (k^* + 1) \leq i \leq n, \end{cases} \end{aligned} \quad (18)$$

where  $F$  is a circular distribution with known and common concentration value for all  $\theta_i$  with mean direction  $\mu_1$  under the null hypothesis  $H_{0m}$  but with two different values  $\mu_1 \neq \mu_2$  under the alternative hypothesis  $H_{1m}$ .

Using Definition-5 we get the estimated curved variance of the data as

$$\bar{b}(0) = \frac{1}{n} \sum_{i=1}^n A_C^{(0)}[(\theta_i - \hat{\mu}_0) \bmod 2\pi], \quad (19)$$

where  $\hat{\mu}_0$  is the estimated circular mean direction of the data  $\theta_1, \theta_2, \dots, \theta_n$ .

Next, we split the data for each possible location  $2 \leq k \leq (n-1)$  and calculate the estimated circular mean for each pair of partitions. Let the mean direction of  $(\theta_1, \theta_2, \dots, \theta_k)$ , and  $(\theta_{k+1}, \theta_{k+2}, \dots, \theta_n)$ , be  $\hat{\mu}_{1k}$ , and  $\hat{\mu}_{2k}$ , respectively. Now, using the Equation-10, we calculate the corresponding areas of the mean shifted angles as

$$b_{ki} = \begin{cases} A_C^{(0)}[(\theta_i - \hat{\mu}_{1k}) \bmod 2\pi] & , \text{ for } i = 1, 2, \dots, k \\ A_C^{(0)}[(\theta_i - \hat{\mu}_{2k}) \bmod 2\pi] & , \text{ for } i = k+1, \dots, n, \end{cases} \quad (20)$$

Let us define  $\bar{b}(k) = \frac{1}{n} \sum_{i=1}^n b_{ki}$  for all  $2 \leq k \leq (n-1)$ . We propose the estimate of the location of the changepoint as

$$k_{max} = \arg \max_k \begin{cases} \frac{\bar{b}(0)}{\bar{b}(k)} & \text{for } 2 \leq k \leq (n-1) \\ 0 & \text{for } k = 1, n. \end{cases} \quad (21)$$

Now, we define the test statistic for the testing problem defined in Equation-18

$$S_n = -2 \log \left( \frac{LR_0}{LR_{1k_{max}} \cdot LR_{2k_{max}}} \right), \quad (22)$$

where,

$$LR_0 = \prod_{i=1}^n f_{\hat{\mu}_0}(\theta_i), \quad LR_{1k_{max}} = \prod_{i=1}^{k_{max}} f_{\hat{\mu}_{1k_{max}}}(\theta_i),$$

and

$$LR_{2k_{max}} = \prod_{j=k_{max}+1}^n f_{\hat{\mu}_{2k_{max}}}(\theta_j),$$

with  $\hat{\mu}_{1k_{max}}$ , and  $\hat{\mu}_{2k_{max}}$  being the estimated circular mean of  $(\theta_1, \theta_2, \dots, \theta_{k_{max}})$ , and  $(\theta_{k_{max}+1}, \theta_{k_{max}+2}, \dots, \theta_n)$  respectively. Under the assumption that the concentration parameter of the distribution is known, using Equation-22, for the CVMC test we

$$\text{Reject } H_{0g}, \text{ if } S_n > s_\alpha, \quad (23)$$

at level  $\alpha$ , where  $s_\alpha$  is the upper  $\alpha$  point of the exact (or asymptotic) distribution of  $S_n$ .

**3.3. Changepoint detection- The general case.** Let  $\theta_1, \theta_2, \dots, \theta_n \in [0, 2\pi)$  be independent angular random variables. We consider the following testing problem :

$$\begin{aligned} H_{0g} &: \theta_i \stackrel{\text{i.i.d.}}{\sim} F(\theta; \boldsymbol{\xi}_1) \text{ for all } i = 1, 2, \dots, n, \\ H_{1g} &: \begin{cases} \theta_i \stackrel{\text{i.i.d.}}{\sim} F(\theta; \boldsymbol{\xi}_1) & , 1 \leq i \leq k^* \\ \theta_i \stackrel{\text{i.i.d.}}{\sim} F(\theta; \boldsymbol{\xi}_2) & , (k^* + 1) \leq i \leq n, \end{cases} \end{aligned} \quad (24)$$

where  $\boldsymbol{\xi}_1, \boldsymbol{\xi}_2$  are suitable vector valued parameters and  $\boldsymbol{\xi}_1 \neq \boldsymbol{\xi}_2$ . under the alternative hypothesis  $H_{1g}$ .

Using the Equation-10, we consider the corresponding non-centered and centered areas on the surface of a curved torus  $\tilde{a}_i = [2(\delta_{(\theta_i < \pi)} - 0.5)] A_C^{(0)}(\theta_i)$  and  $\hat{a}_i = A_C^{(0)}[(\theta_i - \hat{\mu}) \bmod 2\pi]$ , respectively, where  $\hat{\mu}$  is the estimated circular mean of the entire sample and  $[2(\delta_{(\theta_i < \pi)} - 0.5)]$  is an associated sign to the angle  $\theta_i$  for  $i = 1, 2, \dots, n$ . Now, let  $d_i = \max\{\hat{a}_i, \tilde{a}_i\}$  for  $i = 1, 2, \dots, n$ , and

$$S_d^2 = \frac{1}{n-1} \sum_{i=1}^n (d_i - \bar{d})^2,$$

where  $n\bar{d} = \sum_{i=1}^n d_i$ . Now, we define the CUSUM process as

$$U(k) = \frac{1}{n S_d^2} \left[ \sum_{i=1}^k d_i - k\bar{d} \right]^2 \text{ for all } k = 1, \dots, n \quad (25)$$

and define the test statistic

$$\mathcal{G}_n = \max_{1 \leq k < n} \frac{U(k)}{\sqrt{\frac{k}{n} \left(1 - \frac{k}{n}\right)}}. \quad (26)$$

Here, we reject the null hypothesis,  $H_{0g}$ , if  $\mathcal{G}_n > g_\alpha$ , where,  $g_\alpha$  is the upper  $\alpha$  point of the distribution of  $\mathcal{G}_n$  under the null hypothesis. It can be seen from the simulation results reported in Figure-13 that the asymptotic null distribution is close to the distribution of  $B_\infty$ . Hence we propose to obtain the cut-off value  $g_\alpha$  from the distribution of  $B_\infty$  for large  $n$ . Thus, for the SAGC test we

$$\text{Reject } H_{0g} \text{ if } g_\alpha < \mathcal{G}_n. \quad (27)$$

The performance of this test is studied through extensive simulation in Section-4.

**Remark 6.** If there exists more than one changepoint in the given sequence of the data, we can iteratively use the proposed methods to detect these changepoints. The binary segmentation scheme may be used in which the test is applied to each segment, beginning with the full sequence, and depending on the observed p-values, re-segmentation of the data sequence is performed to detect the possible changepoints.

#### 4. NUMERICAL STUDIES

A comprehensive simulation study was conducted first to detect the changepoint in the concentration, then to detect the changepoint in the mean direction, and finally for both. To do so, we have considered the von Mises distribution with the probability distribution function

$$f_{vm}(\theta) = \frac{e^{\kappa \cos(\theta - \mu)}}{2\pi I_0(\kappa)}, \quad (28)$$

where  $0 \leq \theta < 2\pi$ ,  $0 \leq \mu < 2\pi$ ,  $\kappa > 0$ , and  $I_0(\kappa)$  is the modified Bessel function with order zero evaluated at  $\kappa$ .

The Figure-2(A) displays density plot of the test statistic,  $\Lambda_n$  under  $H_{0c}$  with the sample size of  $n = 1000$  from von Mises distribution with mean  $\mu = 0$ , and different concentration parameters,  $\kappa = 0.5, 1, 1.5, 2, 4, 10$ . The number of iterations for each specification is conducted  $5 \times 10^3$  number of times. It is evident from Figure-2 that the densities of the test statistic for different concentration parameters are nearly identical and these are close to the density of the limiting distribution of the random variable  $B_\infty$  (Equation-15). Grabovsky and Horváth (2001) provide a test statistic for testing  $H_{0c}$  against  $H_{1c}$ . They proved that the limiting distribution of the test statistic is the same as that of the random variable

$$\Delta_\infty = \sup_{0 < t < 1} \left[ \frac{B_1^2(t) + B_2^2(t)}{t(1-t)} \right]^{\frac{1}{2}},$$

where  $B_1(t), B_2(t)$  are independent standard Brownian bridges on  $[0, 1]$  if  $\mu = 0$  known.

In Figure-3(A) & 3(B), the distribution of the estimated location of the changepoint and the histogram of the SACC test statistic,  $\Lambda_n$  (Equation-13) are presented under the null hypothesis,  $H_{0c}$ , respectively. We conducted  $5 \times 10^3$  iterations using random samples from the von Mises distribution with a sample size of  $n = 500$ , mean  $\mu = 0$ , and concentration parameter  $\kappa = 1$ . In Figure-3(B) the 90th, 95th, and 99th percentiles are denoted by the vertical lines from left to right, respectively. In Table-1 we provide the cut-off values of the test statistic  $\Lambda_n$  under the null hypothesis,  $H_{0c}$  when the sample of size of 50, 100, 200, 500, and 1000 are drawn from von Mises distribution with mean direction  $\mu = 0$ , and different

concentrations parameters  $\kappa = 0.5, 1, 1.5, 2, 4$  and  $10$ . The table also provides the cut-off values from the limiting distribution of  $B_\infty$  (Equation-15) with the grid size of  $50, 100, 200, 500$ , and  $1000$ , respectively and they are denoted as  $B_\infty^{(n)}$  in general.

The power computation of the SACC test has been summarised in the Algorithm-1. Under the alternative hypothesis,  $H_{1c}$ , the Figure-4(A) & 4(B) show the distribution of the estimated location of the changepoint and the histogram of the SACC test statistic,  $\Lambda_n$  (Equation-13), respectively. Here also, the random samples are drawn from the von Mises distribution with a sample size of  $n = 500$ , mean  $\mu = 0$ . The concentration parameter is  $\kappa_1 = 1$  before the true changepoint  $k^* = \frac{n}{2}$ , and  $\kappa_2 = 0.5$  after the changepoint.

The Figures-5, & 6 provide a comparison of the power of the SACC test (17) with that provided by Grabovsky and Horváth (2001) for sample sizes of  $100$ , and  $500$ , respectively. We consider two levels of significance namely  $1\%$ , and  $5\%$ , and under the null hypothesis,  $\kappa_1 = 2.5$  and under the alternative hypothesis the location of changepoint is considered at  $k^* = \frac{n}{2}$ . The figures are based on  $5 \times 10^3$  iterations. We see from the figures that the power of the SACC test is greater than that of the test given by Grabovsky and Horváth (2001).

The Kato-Jones distribution is a four-parameter family of circular distributions introduced in Kato and Jones (2010). The von Mises and Wrapped Cauchy distributions are members of this general family and it has found some real-life applications. The pdf of the Kato-Jones distribution is

$$f_{kj}(\theta) = \frac{1 - \rho^2}{2\pi I_0(k)} \exp \left[ \frac{\kappa \{ \xi \cos(\theta - \eta) - 2\rho \cos \nu \}}{1 + \rho^2 - 2\rho \cos(\theta - \gamma)} \right] \times \frac{1}{1 + \rho^2 - 2\rho \cos(\theta - \gamma)}, \quad (29)$$

where  $0 \leq \mu, \nu < 2\pi$ , and  $0 \leq \rho < 1$ ,  $\kappa > 0$ , and  $\gamma = \mu + \nu$ ,  $\xi = \sqrt{\rho^4 + 2\rho^2 \cos(2\nu) + 1}$ ,  $\eta = \mu + \arg(\rho^2 \cos(2\nu) + 1 + i\rho^2 \sin(2\nu))$ . Here,  $\mu$  and  $\nu$  are location and  $\kappa$  and  $\rho$  are concentration parameters.

In Figures-7 & 8 we examine the power of the SACC test (17) with that of Grabovsky and Horváth (2001) for the Kato-Jones distribution. We consider a sample size of  $500$  and use the limiting distribution  $B_\infty$  to obtain the cutoff value for the SACC test. Under the null hypothesis,  $H_{0c}$ , we take  $\mu = \nu = 0$ ,  $\rho = 0.4$ , and  $\kappa = 2.5$ . In Figure-7 we keep  $\rho$  fixed and vary  $\kappa$  whereas in Figure-8 we keep  $\kappa$  fixed and vary  $\rho$  to obtain the power functions. We observe from these figures that the SACC test (17) has substantially better power than that of Grabovsky and Horváth (2001).

In Figures-9(A) & 9(B), the distribution of the estimated location of the changepoint and the histogram of the CVMC test statistic,  $S_n$  (Equation-22) are provided, respectively. These figures correspond to the null hypothesis,  $H_{0m}$ , and we conducted  $5 \times 10^3$  iterations using the

random data from the von Mises distribution with a sample size of  $n = 500$ , mean  $\mu = \frac{\pi}{2}$ , and concentration parameter  $\kappa = 1$ . In Figure-9(B) the 90th, 95th, and 99th percentiles are denoted by the vertical lines from left to right, respectively. Table-2 displays the cut-off values for the CVMC test statistic  $S_n$  under the null hypothesis,  $H_{0m}$ . The sample size is fixed at 500, and the data is drawn from a von Mises distribution with mean directions  $\mu = 0, \frac{\pi}{2}$ , and  $\pi$ , each corresponding to different concentration parameters  $\kappa = 0.5, 1$ , and  $1.5$ . In addition to that, the cut-off values of the CVMC test statistic  $S_n$  under the null hypothesis,  $H_{0m}$  when the sample of size of 50, 100, 500 are drawn from von Mises distribution with mean directions  $\mu = 0$ , and different concentrations parameters  $\kappa = 0.5, 1, 1.5, 2, 4, 10$ , are reported in Table-3. Also, the way to obtain the null distribution of the proposed method (CVMC test) has been summarised in the Algorithm-2.

Under the alternative hypothesis, Figures-10(A) & 10(B) depict the distribution of the estimated location of the changepoint and the histogram of the test statistic,  $S_n$  (Equation-22), respectively. Here also, the random sample of size  $n = 500$  follows the von Mises distribution with the concentration parameter  $\kappa = 1$ . The mean direction is  $\mu_1 = \frac{\pi}{2}$  before the true changepoint occurring at  $k^* = \frac{n}{2}$ , and  $\mu_2 = \frac{5\pi}{6}$  after the true changepoint.

Figure-11 depicts the power curve comparison between the CVMC test statistic  $S_n$  and the test statistic  $\Lambda$  from Ghosh et al. (1999) at the level of 1% and 5%, . For each of the levels,  $5 \times 10^3$  iterations have been performed with the sample size of  $n = 500$  from von Mises distribution with the concentration parameter  $\kappa = 1$ , and equispaced mean differences  $\frac{\pi}{12} \leq (\mu_2 - \mu_1) \leq \frac{9\pi}{12}$ , and the true changepoint is at  $k^* = \frac{n}{2}$ . From Figure-11, we can see that the power curves are almost the same. The advantage of the CVMC test (Equation-23) is that we need to compute the value of the likelihood only once, and it is easily extendable to any other circular distributions, even when the evaluation of the maximum likelihood is computationally expensive. For example, we consider the wrapped-Cauchy distribution, a well-known circular distribution having the following probability density function.

$$f_{wc}(\theta) = \frac{1}{2\pi} \frac{1 - \rho^2}{1 + \rho^2 - 2\rho \cos(\theta - \mu)}, \quad (30)$$

where  $0 \leq \theta < 2\pi$ ,  $0 \leq \mu < 2\pi$ , and  $0 \leq \rho < 1$ . Figure-12 portrays the power curves at the levels of 1% and 5% with the sample of size  $n = 500$  from wrapped-Cauchy distribution with the concentration parameter  $\rho = 0.6$ , and equispaced mean differences  $\frac{\pi}{18} \leq (\mu_2 - \mu_1) \leq \frac{\pi}{2}$ , and the true changepoint is at  $k^* = \frac{n}{2}$ . Table-4 displays the cut-off values for the CVMC test (23) under the null hypothesis,  $H_{0m}$ . The sample size is fixed at 500, and the data are drawn from wrapped Cauchy distribution with mean directions  $\mu = 0, \frac{\pi}{2}$ , and  $\pi$ , each corresponding to different concentration parameters  $\rho = 0.3, 0.5$ , and  $0.8$ .



The Figure-13 displays density plot of the test statistic,  $\mathcal{G}_n$  under  $H_{0g}$  with the sample size of  $n = 1000$  from von Mises distribution with the following pairs of parameter specifications:  $(\mu, \kappa) = (0, 0.5), (0, 1), (\frac{\pi}{6}, 1.5), (\frac{\pi}{6}, 2), (\frac{\pi}{3}, 4), (\frac{\pi}{3}, 10)$ . Here we have performed  $5 \times 10^3$  number of iterations for each of the parameter specifications. It is evident from Figure-13 that the densities for different parameter specifications are not only nearly identical but are close to the density of the limiting distribution of the random variable  $B_\infty$  (Equation-15). A binary segmentation scheme (Remark 6) for changepoint detection in either or both the parameters of von Mises distribution with a sample size of 500 has been illustrated in Figure-14. For a pre-specified set of existing changepoints at 125 ( $\mu = \pi$  to  $\mu = \pi/2$ ), 250 ( $\kappa = 0.5$  to  $\kappa = 2$ ), and 375 ( $\mu = \pi/2, \kappa = 2$  to  $\mu = \pi, \kappa = 4$ ) are estimated using the proposed method of SAGC test (Algorithm-3) at 129, 238, and 375 respectively.

## 5. DATA ANALYSIS

In this section, we apply the newly developed procedures to real-life data sets coming from biology, engineering, and meteorology. In Section 5.1 we introduce a new plotting technique for exploratory analysis of temporally ordered angular data that is helpful for changepoint analysis. In the following three Sections 5.2, 5.3 and 5.4 we discuss the changepoint analysis of three real-life data sets and when available, compare the findings with that of the existing procedure.

**5.1. Circular Temporal Plot.** A new scatter plot that we call the *Circular Temporal Plot* is developed to visualize the temporarily ordered angular data. Suppose we have  $n$  temporally ordered angular observations  $\theta_1, \dots, \theta_n$ . Let us begin by considering  $n$  concentric circles with the innermost circle representing time index 1, the next circle representing time index 2, etc. with the outermost circle representing time index  $n$ . The radius of the  $i$ -th circle is taken to be  $\frac{i}{n}R$  where  $R$  is the radius of the outermost circle. The observation  $\theta_i$  is plotted on the  $i$ -th circle as  $\frac{i}{n}R(\cos \theta_i, \sin \theta_i)$ . In the presence of changepoint(s) in the mean direction we expect to see abrupt change(s) in the direction of the plotted observations. Abrupt change(s) in the spread of the plotted observations without a change in direction is indicative of the presence of changepoint(s) in concentration. If both kinds of changes are present we expect to see a combination of the behaviors of the above two situations in the plotted data. The use of this plot is seen to be very helpful in the preliminary analysis of the data and in identifying the appropriate technique to be used for formal analysis. The plot can be further embellished with highlighted circles that segregate the homogeneous segments within annular regions, post the formal analysis of the data using an appropriate procedure. The mean direction of each homogeneous segment is plotted as a point on the highlighted circle corresponding to the outer end of the segment. A proportionate color intensity scale is used to depict the

concentration of the segment. We have implemented the Circular Temporal Plot for the three data sets mentioned above (see Figure-16,18, & 20).

**5.2. Acrophase Data:** We first analyze the Acrophase data set referred by Lombard et al. (2017) by our proposed method (SACC test) as well as by the method of Grabovsky and Horváth (2001). In the context of circadian rhythms, the acrophase represents the time of day at which a particular rhythm reaches its peak. Systolic blood pressure (SBP) exhibits a circadian rhythm. In most people, SBP tends to be lower during periods of rest and sleep, and it increases upon waking and throughout the day. To monitor the acrophase, for SBP, typically, the ambulatory blood pressure monitoring (ABPM) method is used. Tracking the acrophase can serve as an automated early warning system for potential medical conditions before they manifest clinically. The data set contains 306 observations from ambulatory monitoring equipment worn by a patient experiencing episodes of clinical depression, and it is measured in radians in  $[-\pi, \pi]$  that we have converted to data in  $[0, 2\pi]$ .

We have implemented both methods to identify the changepoint in concentration through testing. The binary segmentation procedure (Remark-6) has identified multiple changepoints. The findings and p-value have been reported in Table-5, whereas Table-6 displays the estimated value of the concentration for each of the segments. The p-values have been computed with respect to the limiting distributions  $B_\infty^{(300)}$ . Note that if two successive changepoints are detected within five observations then no further analysis has been done in that short segment. Figure-15 illustrates the estimated location of the changepoints in the concentration by both methods. We also represent the data using a circular temporal plot in Figure-16 where five annular circles from the center to outward represent the corresponding estimated changepoint in the concentration by the proposed method (SACC test).

**5.3. Flare Data:** Lombard (1986) conducted a retrospective analysis of data derived from evaluating illumination flares commonly used in rescue operations, aiming to identify changepoints. The data set consists of a total of 60 angular observations measured in radians within the range  $[-\pi, \pi]$ . To facilitate the proposed method, the data has been transformed to the  $[0, 2\pi]$  interval. The Watson test, at a 5% significance level, indicates adherence to the von Mises distribution. The estimation of the concentration parameter is employed for testing changepoints in the mean direction. Initially, the entire data set (segments 1-60) undergoes testing for changepoints in the mean direction. The results unveil a significant changepoint at the 42nd location, with a p-value of 0.0998 at a 10% significance level using the CVMC test. However, the method by Ghosh et al. (1999) fails to reject the null hypothesis,  $H_{0m}$  with a p-value of 0.5262. Further, the test is conducted on the segment 1 – 42, revealing a changepoint at the 12th location with a p-value of 0.0024 at a 10% significance level. The

test proposed by Lombard (1986) also identifies changepoints at the 12th and 42nd locations that are consistent with the locations identified by the CVMC test. For the graphical representation, readers can refer to Figure-17. We also represent the data using a circular temporal plot in Figure-18 where two annular circles from the center to outward represent the corresponding estimated changepoint in the mean direction by the proposed method. The segment-wise estimated mean is represented by red bubble plot at the outer end corresponding segment.

**5.4. Amphan Cyclone Data:** The Super Cyclonic Storm (SuCS) “AMPHAN” that caused extensive damage to eastern India and Bangladesh occurred during the period 16th May 2020 to 21st May 2020 over the Bay of Bengal (BoB). As per the description by the Regional specialized meteorological center - tropical cyclones, New Delhi India Meteorological Department (see, [https://internal.imd.gov.in/press\\_release/20200614\\_pr\\_840.pdf](https://internal.imd.gov.in/press_release/20200614_pr_840.pdf)), AMPHAN started forming from the remnant of a low-pressure area that occurred over the south Andaman Sea and adjoining southeast Bay of Bengal during the period 6th-12th May 2020. This gradually developed into a well-marked low-pressure area that was observed over south-east BoB at 0300 UTC on 14th May 2020. It intensified into a cyclonic storm over southeast BoB on the 16th of May 2020. This further intensified into a SuCS over the next two and half days and maintained the intensity of SuCS for nearly 24 hours, before weakening into an Extremely Severe Cyclonic Storm over west-central BoB on 19th May 2020 and made landfall at  $21.65^{\circ}N, 88.3^{\circ}E$  on the coast of West Bengal, India during 1000-1200 UTC on 20th May, with a maximum sustained wind speed of 155 – 165 kmph gusting to 185 kmph.

Intending to study the possible association of the wind direction at a chosen location with the meteorological events described above, we collected the 10-meter-above-the-sea-level wind direction data (see Hersbach et al., 2023) at the location with coordinates  $11^{\circ}N$ , and  $86.5^{\circ}E$ , which is about 1200 km from the location of the landfall. The hourly data spans from May 10, 2020, 0000 UTC to May 20, 2020, 1200 UTC. This resulted in a total of 258 observations reported in degrees.

As discussed above, several significant meteorological events happened during the period 10th - 20th May 2020 which indicates the possibility of changepoint(s) being present in the data. Since both the mean direction and the concentration are unknown, we executed the SAGC test described in Algorithm- 3, to determine the existence of changepoint(s) for concentration and/or mean direction, in this data set. Using the binary segmentation procedure (6) we found the presence of multiple changepoints. Table-7 reports the results, whereas Table-8 shows the estimated values of the concentration and mean direction for each segment. It may be noted that we used the limiting distributions  $B_{\infty}^{(258)}$ , to obtain the corresponding p-values. Also, note that if two successive changepoints are detected in a

short range (less than 24 hours) then further analysis has not been carried out in that short segment.

It is interesting to observe that the changepoints detected at locations 47 (1730 UTC, 11 May 2020) and 69 (1530 UTC, 12 May 2020) correspond to the manifestation of a low-pressure area over the South Andaman Sea and adjoining southeast BoB. The changepoint at location 103 (0130 UTC, 14 May 2020) is the identification of a well-marked low-pressure area over southeast BoB reported at 0300 UTC on 14th May 2020. Moreover, changepoints at locations 156 (0630 UTC, 16 May 2020) and 168 (1830 UTC, 16 May 2020) correspond to the occurrence of a deep depression reported at 0900 UTC on 16th May, which subsequently intensified into a cyclonic storm later in the same day. The final changepoint was detected before landfall at location 235 (1330 UTC, 19 May 2020). Thus we see that the estimated locations of these changepoints closely correspond to meteorological phenomena associated with the Super Cyclonic Storm. Figure-19 depicts the changepoint locations estimated by the proposed method (Algorithm- 3). We also represent the data using a circular temporal plot in Figure-20 where eight annular circles from the center to outward represent the corresponding estimated changepoints in the mean direction or/and concentration by the proposed method. The segment-wise estimated mean is represented by red bubble plot at the outer end corresponding segment.

## 6. CONCLUSION

In this paper, a new notion of the “square of an angle” has been introduced by using the intrinsic geometry of a curved torus. This makes it possible for us to define “curved variance”, a new measure of variation analogous to the concept of variance, for angular random variables. Separate analyses of changepoint problems in concentration, mean direction, and/or both are developed with the help of the above notions. The null distribution of the SACC test statistic for identifying the changepoint in the concentration is found to be asymptotically invariant with respect to the underlying concentration and mean direction. The simulation results show that the proposed test is more powerful than the existing one. For detecting changepoints in the mean direction a new test has been developed using “curved variance” and the likelihood ratio together. Extensive simulation shows that it performs at par with the existing test for von Mises distribution with known concentration parameters. The CVMC test is easily extendable to other circular distributions. When changepoints are present in either the mean direction or the concentration the SAGC test is seen to provide desirable performance. The tests are applied to three real-life data sets and are seen to provide useful insights.

## REFERENCES

- A. Anastasiou and A. Papanastasiou. Generalized multiple change-point detection in the structure of multivariate, possibly high-dimensional, data sequences. *Statistics and Computing*, 33(5):94, 2023.
- J. Antoch, M. Husková, and Z. Prásková. Effect of dependence on statistics for determination of change. *Journal of Statistical Planning and Inference*, 60:291–310, 1997.
- B. Banerjee and S. Mazumder. A more powerful test identifying the change in mean of functional data. *Annals of the Institute of Statistical Mathematics*, 70:691–715, 2018.
- B. Banerjee, A. K. Laha, and A. Lakra. Data-driven dimension reduction in functional principal component analysis identifying the change-point in functional data. *Statistical Analysis and Data Mining: The ASA Data Science Journal*, 13(6):529–536, 2020.
- P. Billingsley. *Convergence of probability measures*. John Wiley & Sons, 2013.
- G. Cobb. The problem of the Nile: Conditional solution to a change-point problem. *Biometrika*, 65:243–251, 1978.
- R. Davis, D. Huang, and Y.-C. Yao. Testing for a change in the parameter values and order of an autoregressive model. *The Annals of Statistics*, 23:282–304, 1995.
- P. Fearnhead and G. Rigai. Changepoint detection in the presence of outliers. *Journal of the American Statistical Association*, 114(525):169–183, 2019.
- J. Gallier and J. Quaintance. *Differential Geometry and Lie Groups: A Computational Perspective*. Springer, 2020.
- K. Ghosh, S. R. Jammalamadaka, and M. Vasudaven. Change-point problems for the von mises distribution. *Journal of Applied Statistics*, 26(4):423–434, 1999.
- I. Grabovsky and L. Horváth. Change-point detection in angular data. *Annals of the Institute of Statistical Mathematics*, 53:552–566, 2001.
- K. Haynes, P. Fearnhead, and I. A. Eckley. A computationally efficient nonparametric approach for changepoint detection. *Statistics and computing*, 27:1293–1305, 2017.
- H. Hersbach, B. Bell, P. Berrisford, G. Biavati, A. Horányi, J. Muñoz Sabater, C. Nicolas, J. and Peubey, R. Radu, I. Rozum, D. Schepers, A. Simmons, C. Soci, D. Dee, and J.-N. Thépaut. Era5 hourly data on single levels from 1940 to present. *Copernicus Climate Change Service (C3S) Climate Data Store (CDS)*, DOI: 10.24381/cds.adbb2d47 (Accessed on 10-January-2023):268–279, 2023. URL <https://cds.climate.copernicus.eu/cdsapp#!/dataset/reanalysis-era5-single-levels?tab=overview>.
- S. Hörmann and P. Kokoszka. Weakly dependent functional data. *The Annals of Statistics*, 38(3):1845–1884, 2010. ISSN 0090-5364. doi: 10.1214/09-AOS768. URL <http://dx.doi.org/10.1214/09-AOS768>.
- L. Horváth and P. Kokoszka. *Inference for functional data with applications*, volume 200. Springer Science & Business Media, 2012.
- L. Horváth, P. Kokoszka, and J. Steinebach. Testing for changes in multivariate dependent observations with applications to temperature changes. *Journal of Multivariate Analysis*, 68:96–119, 1999.
- S. R. Jammalamadaka and A. Sengupta. *Topics in circular statistics*, volume 5. world scientific, 2001.
- S. Kato and M. Jones. A family of distributions on the circle with links to, and applications arising from, Möbius transformation. *Journal of the American Statistical Association*, 105(489):249–262, 2010.
- C. Kirch, B. Muhsal, and H. Ombao. Detection of changes in multivariate time series with application to EEG data. *Journal of the American Statistical Association*, 110(511):1197–1216, 2015.
- P. Kokoszka and R. Leipus. Change-point estimation in ARCH models. *Bernoulli*, 6:513–539, 2000.
- F. Lombard. The change-point problem for angular data: A nonparametric approach. *Technometrics*, 28(4):391–397, 1986.
- F. Lombard, D. M. Hawkins, and C. J. Potgieter. Sequential rank cusum charts for angular data. *Computational Statistics & Data Analysis*, 105:268–279, 2017. URL <http://dx.doi.org/10.1016/j.csda.2016.08.001>.
- K. V. Mardia. *Directional statistics*. New York: John Wiley and Sons., 2000.

- L. Pishchagina, G. Romano, P. Fearnhead, V. Runge, and G. Rigai. Online multivariate changepoint detection: Leveraging links with computational geometry. *arXiv preprint arXiv:2311.01174*, 2023.
- A. SenGupta and A. K. Laha. A likelihood integrated method for exploratory graphical analysis of change point problem with directional data. *Communications in Statistics-Theory and Methods*, 37(11):1783–1791, 2008.
- X. Shao and X. Zhang. Testing for change points in time series. *Journal of the American Statistical Association*, 105(491):1228–1240, 2010.

## 7. APPENDIX

---

**Algorithm 1:** Power calculation algorithm of the test statistic to detect changepoint in concentration parameters.

---

```

n ∈ ℕ ;                                     /* Sample size */
I ∈ ℕ ;                                     /* Number of iteration, preferably large */
R = r = 1 ;                                 /* R,r are radius of unit circle */
cp ∈ {1, 2, …, (n − 1)} ;                 /* Location of true changepoint */
κ0, κp ∈ (0, ∞) ;                       /* In particular for von misses distribution */
μ ∈ [0, 2π);
for j = 1, 2, …, I do
  θ1, θ2, …, θcp ∼ f(θ, μ, κ0) ;
  θcp+1, θcp+2, …, θn ∼ f(θ, μ, κp) ;
  ai ← AC(0)[(θi − μ) mod 2π] for i = 1, 2, …, n ;
  Var( $\widehat{a}$ ) ←  $\frac{1}{n-1} \sum_{i=1}^n (a_i - \bar{a})^2$ , n $\bar{a}$  =  $\sum_{i=1}^n a_i$ ;
  T(k) ←  $\frac{1}{n \widehat{Var}(a)} \left[ \sum_{i=1}^k a_i - k\bar{a} \right]^2$  for all k = 1, …, n;
  Λn =  $\max_{1 \leq k < n} \frac{T(k)}{\sqrt{\frac{k}{n} \left(1 - \frac{k}{n}\right)}}$ ;
  Re[j] ← δ(Λn > lα) ;                 /* δ is the Dirac delta function */
end
power ←  $\frac{1}{I} \sum_{i=1}^I Re[i]$  ;

```

**Result:** Power of the test can be obtained by varying the concentration parameter  $k_p$  while keeping  $k_0$  fixed.

---

---

**Algorithm 2:** Cut-off calculation algorithm for the test statistic to detect change-point in mean direction, when concentration, is known.

---

```

 $n \in \mathbb{N}$  ; /* Sample size */
 $I \in \mathbb{N}$  ; /* Number of iteration, preferably large */
 $R = r = 1$  ; /* R,r are radius of unit circle */
 $\kappa \in (0, \infty)$  ; /* In particular for von misses distribution */
 $\mu \in [0, 2\pi)$  ;
for  $j = 1, 2, \dots, I$  do
   $\theta_1, \theta_2, \dots, \theta_k, \theta_{k+1}, \dots, \theta_n \sim f(\theta, \mu, \kappa)$  ;
   $\hat{\mu}_0 \leftarrow$  Circular mean of  $(\theta_1, \theta_2, \dots, \theta_n)$ ;
   $\bar{b}(0) \leftarrow \frac{1}{n} \sum_{i=1}^n A_C^{(0)}[(\theta_i - \hat{\mu}_0) \bmod 2\pi]$ ;
  for  $k = 2, \dots, (n-1)$  do
     $\hat{\mu}_{1k} \leftarrow$  Circular mean of  $(\theta_1, \theta_2, \dots, \theta_k)$ ;
     $\hat{\mu}_{2k} \leftarrow$  Circular mean of  $(\theta_{k+1}, \theta_{k+2}, \dots, \theta_n)$ ;
     $b_{ki} \leftarrow \begin{cases} A_C^{(0)}[(\theta_i - \hat{\mu}_{1k}) \bmod 2\pi] & , \text{ for } i = 1, 2, \dots, k \\ A_C^{(0)}[(\theta_i - \hat{\mu}_{2k}) \bmod 2\pi] & , \text{ for } i = k+1, k+2, \dots, n, \end{cases}$ 
     $\bar{b}(k) \leftarrow \frac{1}{n} \sum_{i=1}^n b_{ki}$ ;
  end
   $k_{max} \leftarrow \arg \max_k \left\{ \frac{\bar{b}(0)}{\bar{b}(k)} \right\}$  ; /* Estimated location of changepoint */
   $S_n[j] \leftarrow -2 \log \left( \frac{LR_0}{LR_{1k_{max}} \cdot LR_{2k_{max}}} \right)$ ;
end

```

**Result:**  $s_\alpha \leftarrow (1 - \alpha)$ th quantile of the array  $S_n$ .

---

		Quantiles		
		0.90th	0.95th	0.99th
$n = 50$	$\kappa = 0.5$	2.8664	3.5570	5.1797
	$\kappa = 1$	2.8852	3.4706	4.9647
	$\kappa = 1.5$	2.9324	3.4908	5.1092
	$\kappa = 2$	2.9059	3.5290	4.9475
	$\kappa = 4$	2.9876	3.6723	5.2044
	$\kappa = 10$	3.0115	3.6687	5.1525
	$B_\infty^{(50)}$	2.8967	3.5376	5.0784
$n = 100$	$\kappa = 0.5$	2.9655	3.6087	5.0154
	$\kappa = 1$	2.9998	3.6626	5.1375
	$\kappa = 1.5$	2.9601	3.5823	5.0707
	$\kappa = 2$	3.0054	3.6686	5.1957
	$\kappa = 4$	3.1320	3.8628	5.4352
	$\kappa = 10$	3.0528	3.7376	5.1318
	$B_\infty^{(100)}$	2.9987	3.6939	5.2307
$n = 200$	$\kappa = 0.5$	3.0294	3.6653	5.1041
	$\kappa = 1$	3.0619	3.7477	5.3283
	$\kappa = 1.5$	3.0533	3.7104	5.0903
	$\kappa = 2$	3.1221	3.8160	5.5242
	$\kappa = 4$	3.1010	3.8392	5.1764
	$\kappa = 10$	3.1391	3.8052	5.3281
	$B_\infty^{(200)}$	3.0353	3.6733	5.2212
$n = 500$	$\kappa = 0.5$	3.1820	3.8620	5.3930
	$\kappa = 1$	3.1469	3.9033	5.7212
	$\kappa = 1.5$	3.2189	3.8676	5.4404
	$\kappa = 2$	3.1148	3.8149	5.5284
	$\kappa = 4$	3.0986	3.8050	5.3250
	$\kappa = 10$	3.1611	3.8389	5.4520
	$B_\infty^{(500)}$	3.2224	3.9021	5.7649
$n = 1000$	$\kappa = 0.5$	3.2093	3.9429	5.5770
	$\kappa = 1$	3.2860	3.9551	5.5877
	$\kappa = 1.5$	3.2012	3.9068	5.7190
	$\kappa = 2$	3.2164	3.9404	5.4612
	$\kappa = 4$	3.1152	3.8271	5.4818
	$\kappa = 10$	3.2164	3.9404	5.4612
	$B_\infty^{(1000)}$	3.2173	3.8994	5.3781

TABLE 1. Table of the cut-off values of the SACC test statistic  $\Lambda_n$  under the null hypothesis,  $H_{0c}$  when the sample of sizes of 50, 100, 200, 500, and 1000 are drawn from von Mises distribution with mean direction  $\mu = 0$ , and different concentration parameters  $\kappa = 0.5, 1, 1.5, 2, 4$  and 10. The table also contains the cut-off values from the limiting distribution of  $B_\infty$  (Equation-15) with the grid size of 50, 100, 200, 500, and 1000, respectively.



		Quantiles		
		0.90th	0.95th	0.99th
$\kappa = 0.5$	$\mu = 0$	8.5456	10.0233	13.8042
	$\mu = \frac{\pi}{2}$	8.5492	10.0849	13.7622
	$\mu = \pi$	8.5860	10.0583	13.5162
$\kappa = 1$	$\mu = 0$	8.8183	10.2612	13.0927
	$\mu = \frac{\pi}{2}$	8.6837	10.2731	13.5921
	$\mu = \pi$	8.8742	10.2840	13.8020
$\kappa = 1.5$	$\mu = 0$	8.9328	10.5176	13.9789
	$\mu = \frac{\pi}{2}$	9.2186	10.7631	13.5326
	$\mu = \pi$	9.0382	10.5016	14.3562

TABLE 2. Table of the cut-off values of the CVMC test statistic  $S_n$  under the null hypothesis,  $H_{0m}$  when the sample of size of 500 is drawn from von Mises distribution with different mean directions  $\mu = 0, \frac{\pi}{2}$ , and  $\pi$  and concentration parameters  $\kappa = 0.5, 1$ , and  $1.5$ .

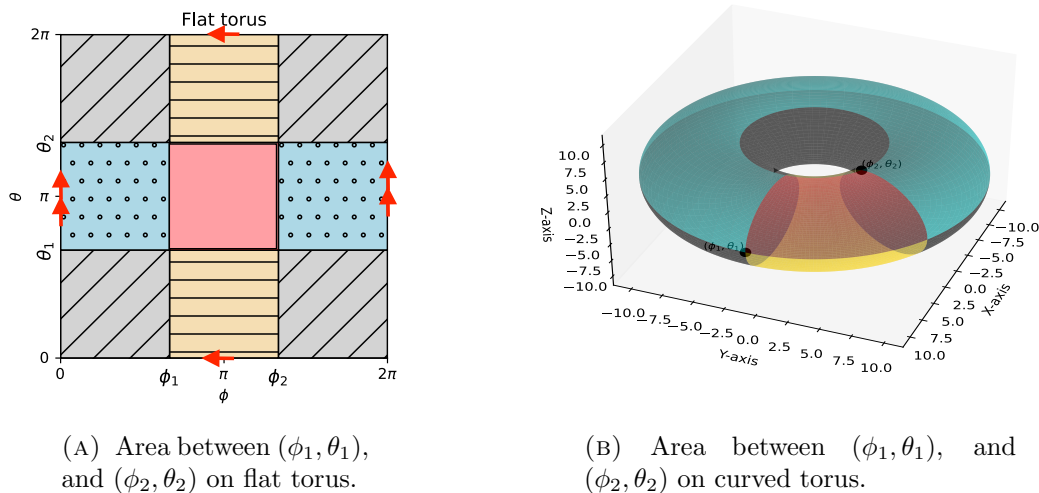


FIGURE 1. Decomposition of the surface area between two points  $(\phi_1, \theta_1)$  and  $(\phi_2, \theta_2)$  (a) on a flat torus and (b) a curved torus.

		Quantiles		
		0.90th	0.95th	0.99th
$n = 50$	$\kappa = 0.5$	6.5722	7.8637	10.2533
	$\kappa = 1$	7.5233	8.9762	12.0100
	$\kappa = 1.5$	7.6742	9.1220	12.2159
	$\kappa = 2$	7.4798	8.9543	12.5480
	$\kappa = 4$	7.2877	8.8327	12.3680
	$\kappa = 10$	7.0852	8.6129	11.9444
$n = 100$	$\kappa = 0.5$	7.4101	8.8300	12.5361
	$\kappa = 1$	8.0260	9.5321	12.8955
	$\kappa = 1.5$	8.2939	9.7830	12.9363
	$\kappa = 2$	8.1398	9.6036	13.2454
	$\kappa = 4$	7.7705	9.2947	13.0220
	$\kappa = 10$	7.7706	9.4081	13.0166
$n = 200$	$\kappa = 0.5$	8.0906	9.5555	12.9020
	$\kappa = 1$	8.3988	9.9724	13.3396
	$\kappa = 1.5$	8.4884	10.0626	13.0109
	$\kappa = 2$	8.5996	10.0631	13.1336
	$\kappa = 4$	8.3216	9.7448	13.3388
	$\kappa = 10$	8.2707	9.8393	13.0018

TABLE 3. Table of the cut-off values of the CVMC test statistic  $S_n$  under the null hypothesis,  $H_{0m}$  when the sample of sizes of 50, 100, 500 are drawn from von Mises distribution with mean directions  $\mu = 0$ , and different concentration parameters  $\kappa = 0.5, 1, 1.5, 2, 4, 10$ .

		Quantiles		
		0.90th	0.95th	0.99th
$\rho = 0.3$	$\mu = 0$	8.5028	9.9692	12.5997
	$\mu = \frac{\pi}{2}$	8.5091	10.0022	13.3221
	$\mu = \pi$	8.6932	10.0872	13.2863
$\rho = 0.5$	$\mu = 0$	8.5504	10.0791	13.5735
	$\mu = \frac{\pi}{2}$	8.3479	9.9118	13.2359
	$\mu = \pi$	8.4932	10.1220	13.9901
$\rho = 0.8$	$\mu = 0$	5.9095	8.4464	13.0573
	$\mu = \frac{\pi}{2}$	5.6248	8.2641	12.7238
	$\mu = \pi$	5.7724	8.1428	12.9080

TABLE 4. Table of the cut-off values of the CVMC test statistic  $S_n$  under the null hypothesis,  $H_{0m}$  when the sample of size of 500 is drawn from wrapped Cauchy distribution with different mean directions  $\mu = 0, \frac{\pi}{2}$ , and  $\pi$  and concentration parameters  $\rho = 0.3, 0.5$ , and  $0.8$ .

Proposed Method			by Grabovsky and Horváth (2001)		
Data segment	Estimated change-point	P-value	Data segment	Estimated change-point	P-value
1-306	248	0.0000	1-306	242	0.000
1-248	116	0.0000	1-242	126	0.0004
1-116	103	0.0000	1-126	103	0.0009
1-103	76	0.1762	1-103	87	0.0020
104-116	105	0.0000	1-87	59	0.1902
117-248	149	0.9593	88-103	91	0.9606
249-306	269	0.0000	104-126	110	0.0036
249-269	264	0.4814	111-126	115	0.0290
270-306	298	0.0372	116-126	124	0.9561
270-298	281	0.5496	127-242	171	0.6903
299-306	302	0.9457	243-306	269	0.0126
			270-306	298	0.0518

TABLE 5. Binary segmentation scheme to detect changepoint in the acrophase data set by the proposed method in the left panel and the method by Grabovsky and Horváth (2001) at the right panel.

Homogeneous segment	1-103	104-116	117-248	249-269	270-298	299-306
Estimated concentrations	0.5598	0.6288	0.7602	0.3799	0.7298	0.4391

TABLE 6. This table represents the value of the concentration parameter for each segment of the estimated location of changepoints.

Data segment	Estimated change point	P-value
1-258	235	0.0000
1-235	103	0.0000
1-103	47	0.0000
1-47	7	0.0008
8-47	26	0.0626
48-103	69	0.0034
70-103	99	0.1158
104-235	168	0.0000
104-168	156	0.0006
104-156	118	0.0006
119-156	138	0.0002
169-235	173	0.0648

TABLE 7. Binary segmentation scheme to detect change point in the cyclone Amphan data set.

Homogeneous range	Mean direction in degrees (radians)	Concentration
1-47	1.79(102.31)	0.9539627
48-69	1.45(83.17)	0.9979347
70-103	1.06(60.48)	0.9339317
104-118	2.19(125.7)	0.9633238
119-138	1.60(91.6)	0.9874869
139-156	1.97(112.88)	0.978662
157-168	2.42(138.77)	0.9729238
169-235	4.12(236.06)	0.9787712
236-258	3.74(214.08)	0.9941826

TABLE 8. This table represents the value of the mean direction in radian(degree) and concentration parameter for each segment of the estimated location of changepoints.

---

**Algorithm 3:** Power calculation algorithm of the test statistic to detect changepoint in mean direction and/or concentration parameters.

---

```

 $n \in \mathbb{N}$  ; /* Sample size */
 $I \in \mathbb{N}$  ; /* Number of iteration, preferably large */
 $R = r = 1$  ; /* R,r are radius of unit circle */
 $cp \in \{1, 2, \dots, (n-1)\}$  ; /* Location of true changepoint */
 $\kappa_0, \kappa_p \in (0, \infty)$  ; /* In particular for von misses distribution */
 $\mu_0, \mu_p \in (0, 2\pi)$  ;
for  $j = 1, 2, \dots, I$  do
   $\theta_1, \theta_2, \dots, \theta_{cp} \sim f(\theta, \mu_0, \kappa_0)$  ;
   $\theta_{cp+1}, \theta_{cp+2}, \dots, \theta_n \sim f(\theta, \mu_p, \kappa_p)$  ;
   $\hat{\mu} \in (0, 2\pi]$  ; /* Estimated circular mean */
   $\tilde{a}_i \leftarrow [2(\delta_{(\theta_i < \pi)} - 0.5)] A_C^{(0)}(\theta_i)$  for  $i = 1, 2, \dots, n$  ;
   $\hat{a}_i \leftarrow A_C^{(0)}[(\theta_i - \hat{\mu}) \bmod 2\pi]$  for  $i = 1, 2, \dots, n$  ;
   $d_i \leftarrow \max_{1 \leq i \leq n} \{\hat{a}_i, \tilde{a}_i\}$  ;

   $\widehat{Var}(d) \leftarrow \frac{1}{n-1} \sum_{i=1}^n (d_i - \bar{d})^2$ ,  $n\bar{d} = \sum_{i=1}^n d_i$ ;

   $U(k) \leftarrow \frac{1}{n \widehat{Var}(d)} \left[ \sum_{i=1}^k d_i - k\bar{d} \right]^2$  for all  $k = 1, \dots, n$ ;

   $\mathcal{G}_n = \max_{1 \leq k < n} \frac{U(k)}{\sqrt{\frac{k}{n} (1 - \frac{k}{n})}}$ ;

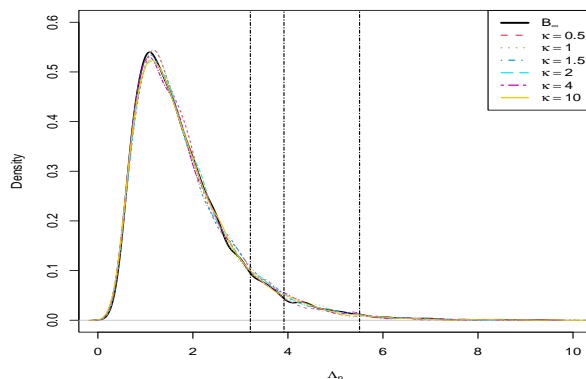
   $Re[j] \leftarrow \delta_{(\mathcal{G}_n > g_\alpha)}$  ; /*  $\delta$  is the Dirac delta function */
end

 $power \leftarrow \frac{1}{I} \sum_{i=1}^I Re[i]$  ;

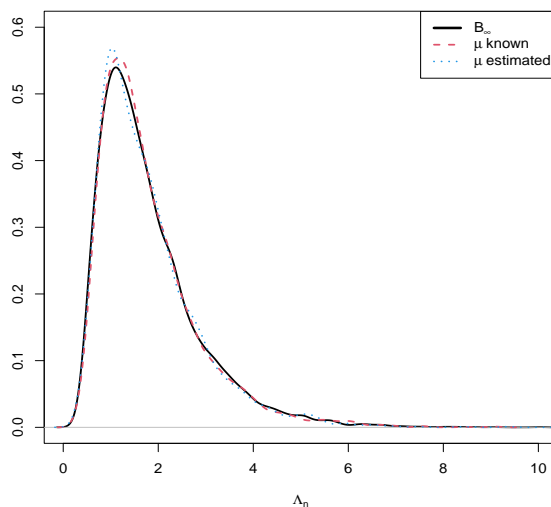
```

**Result:** Power of the test can be obtained by varying the concentration parameter  $k_p$  while keeping  $k_0$  fixed.

---



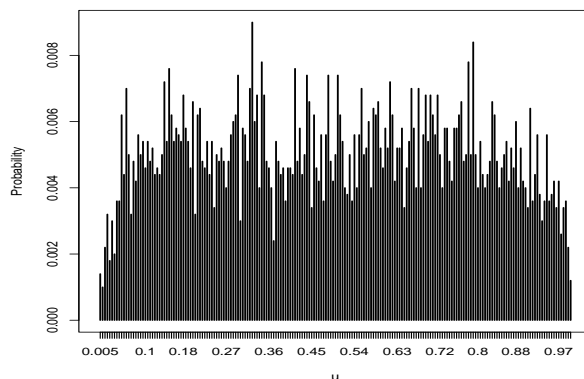
(A) Density plot of the test statistic,  $\Lambda_n$  under  $H_{0c}$  with sample of size  $n = 1000$  from von Mises distribution with the mean  $\mu = 0$ , and different concentration parameters,  $\kappa = 0.5, 1, 1.5, 2, 4, 10$ . Density plot of the limiting random variable  $B_\infty$  along with the 0.90th, 0.95th, and 0.99th quantiles.



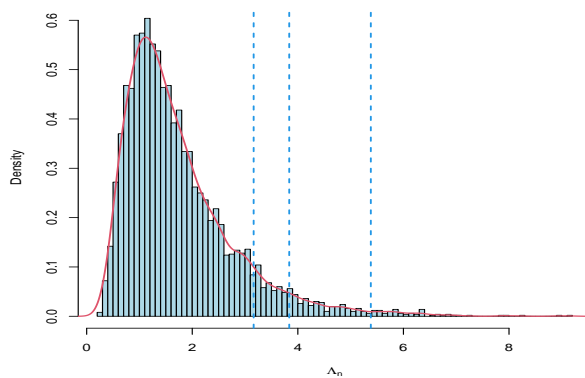
(B) Density plot of the test statistic,  $\hat{\Lambda}_n$  under  $H_{0c}$  with sample of size  $n = 1000$  from von Mises distribution with the mean  $\mu$  is known and  $\mu$  is estimated for the concentration parameter,  $\kappa = 1$  along with the density plot of the limiting random variable  $B_\infty$ .

FIGURE 2. The plots of the distribution of the estimated location of change-point and the SACC test statistic along with the 0.90th, 0.95th, 0.99th quantiles under the null hypothesis,  $H_{0c}$  when the data are from von Mises distribution (sample size  $n = 1000$ ) with concentration parameter,  $\kappa = 1$  and the known mean direction  $\mu = 0$ .



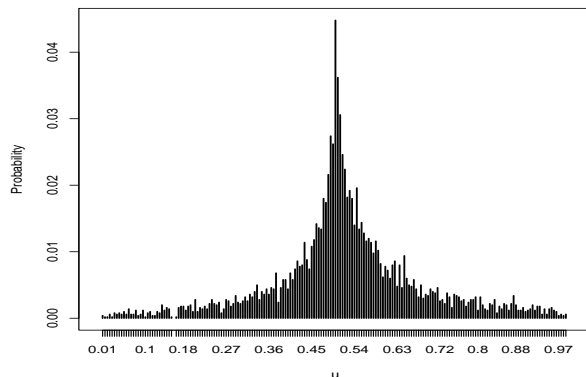


(A) Distribution of estimated location of changepoint in concentration parameter.

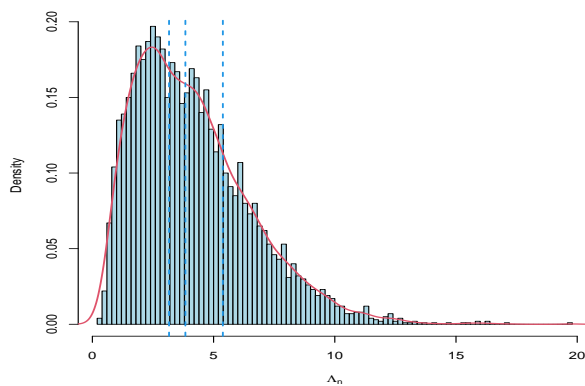


(B) Histogram of  $\Lambda_n$ .

FIGURE 3. The plots of the distribution of the estimated location of changepoint and the SACC test statistic along with the 0.90th, 0.95th, 0.99th quantiles under the null hypothesis,  $H_{0c}$  when the data are from von Mises distribution (sample size  $n = 500$ ) with concentration parameter,  $\kappa = 1$  and the known mean direction  $\mu = 0$ .



(A) Distribution of estimated location of changepoint in concentration parameter.



(B) Histogram of  $\Lambda_n$ .

FIGURE 4. The plots of the distribution of the estimated location of changepoint and that of the SACC test statistic when the true changepoint is at  $k^* = \frac{n}{2}$ ,  $\kappa_1 = 1, \kappa_2 = 0.5$  and mean direction  $\mu = 0$  under the alternative hypothesis,  $H_{1c}$  along with the 0.90th, 0.95th, 0.99th quantiles when the data are from von Mises distribution (sample size  $n = 500$ ) under  $H_{0c}$ .

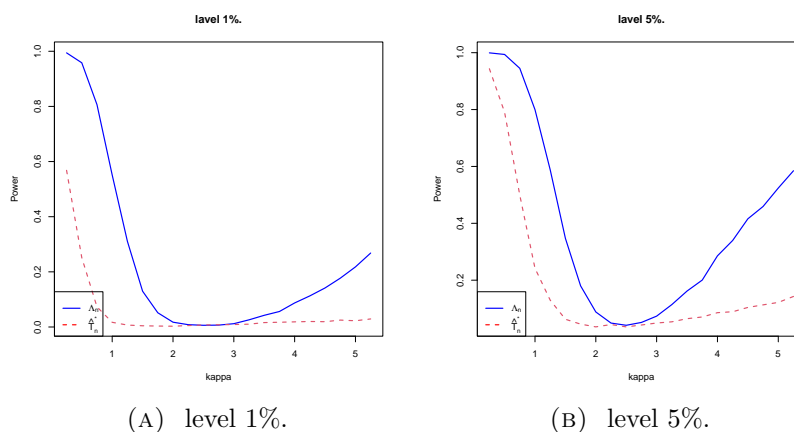


FIGURE 5. Power comparison between  $\Lambda_n$  and  $\widehat{T}_n^*$  with respect to  $\kappa$  for the sample size of  $n = 100$ , drawn from von Mises distribution with true change-point at  $k^* = \frac{n}{2}$  under  $H_{1c}$ . and  $\mu = 0, \kappa = 2.5$  under  $H_{0c}$ .

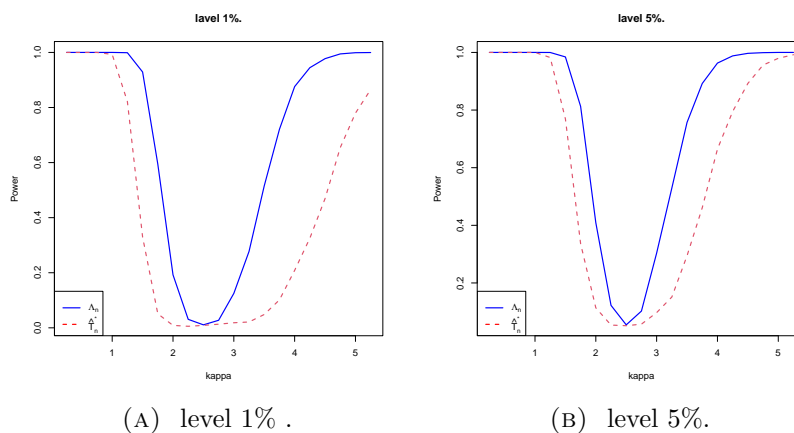


FIGURE 6. Power comparison between  $\Lambda_n$  and  $\widehat{T}_n^*$  with respect to  $\kappa$  for the sample size of  $n = 500$ , drawn from von Mises distribution with true change-point at  $k^* = \frac{n}{2}$  under  $H_{1c}$ . and  $\mu = 0, \kappa = 2.5$  under  $H_{0c}$ .

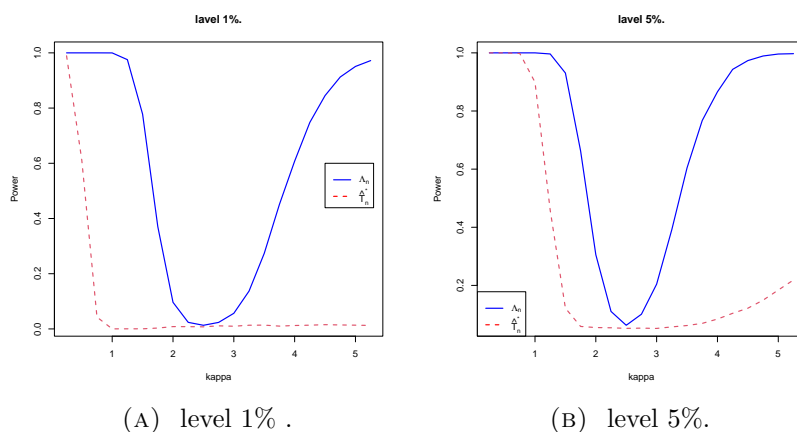


FIGURE 7. Power comparison between  $\Lambda_n$  and  $\widehat{T}_n^*$  with respect to  $\kappa$  for the sample size of  $n = 500$ , when the data are from Kato-Jones distribution with true changepoint at  $k^* = \frac{n}{2}$  under  $H_{1c}$ . and  $\mu = \nu = 0, \rho = 0.4, \kappa = 2.5$  under  $H_{0c}$ .

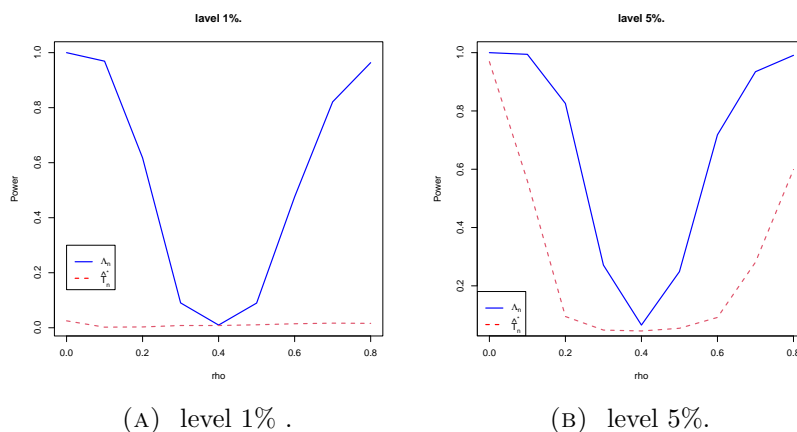
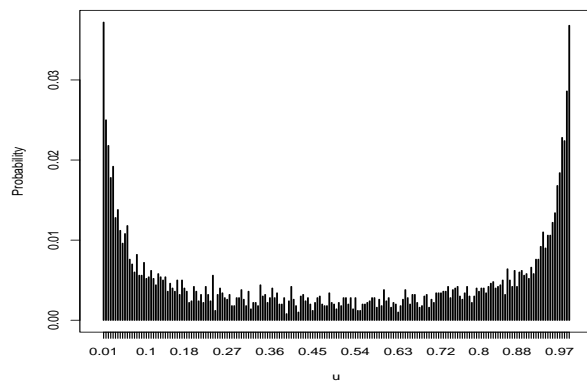
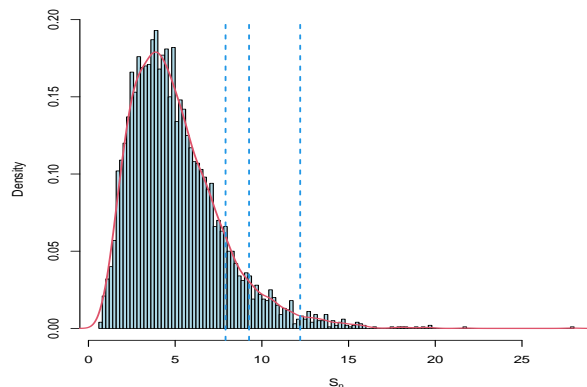


FIGURE 8. Power comparison between  $\Lambda_n$  and  $\widehat{T}_n^*$  with respect to  $\rho$  for the sample size of  $n = 500$ , when the data are from Kato-Jones distribution with true changepoint at  $k^* = \frac{n}{2}$  under  $H_{1c}$ . and  $\mu = \nu = 0, \rho = 0.4, \kappa = 2.5$  under  $H_{0c}$ .

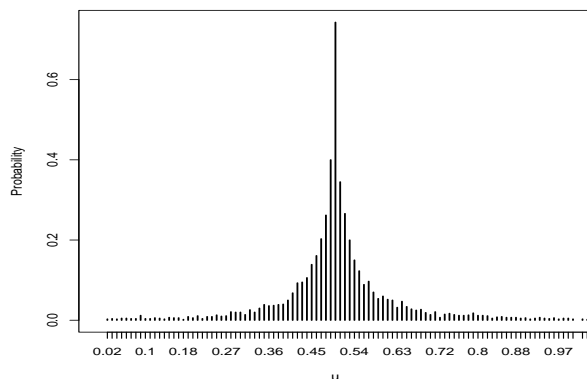


(A) Distribution of estimated location of the changepoint in mean direction.

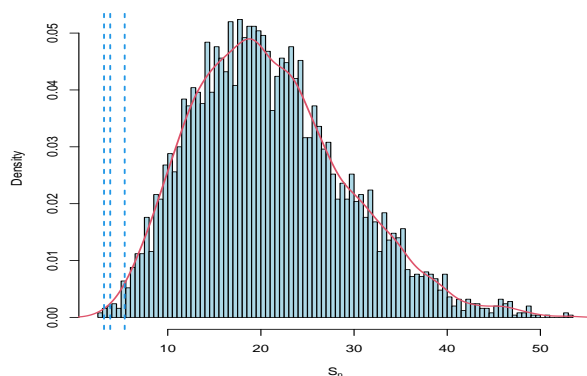


(B) Histogram of  $S_n$ .

FIGURE 9. The plots of the distribution of estimated location changepoint and the CVMC test statistic along with the 0.90th, 0.95th, 0.99th quantiles under the null hypothesis,  $H_{0m}$  when the data are from von Mises distribution (sample size  $n = 500$ ) with known concentration parameter  $\kappa = 1$  and mean direction  $\mu = \frac{\pi}{2}$ .



(A) Distribution of estimated location changepoint in mean direction.



(B) Histogram of  $S_n$ .

FIGURE 10. The plots of the distribution of estimated location changepoint and that of the CVMC test statistic when the true changepoint is at  $k^* = \frac{n}{2}$  under the alternative hypothesis,  $H_{1m}$  along with the 0.90th, 0.95th, 0.99th quantiles when the data are from von Mises distribution (sample size  $n = 500$ ) with mean directions  $\mu_1 = \frac{\pi}{2}, \mu_2 = \frac{5\pi}{6}$ , and known concentration parameter  $\kappa = 1$  under  $H_{0m}$ .

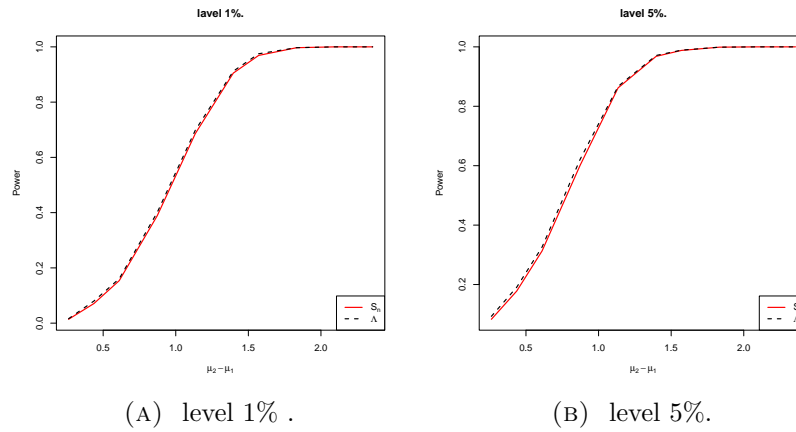


FIGURE 11. Plot of the power functions the CVMC test statistic,  $S_n$  and  $\Lambda$  by Ghosh et al. (1999) for sample of size  $n = 500$  from von Mises distribution with the concentration parameter  $\kappa = 1$ , and equispaced mean differences in  $\frac{\pi}{12} \leq (\mu_2 - \mu_1) \leq \frac{9\pi}{12}$ , with the true changepoint at  $k^* = \frac{n}{2}$  under  $H_{1m}$ .

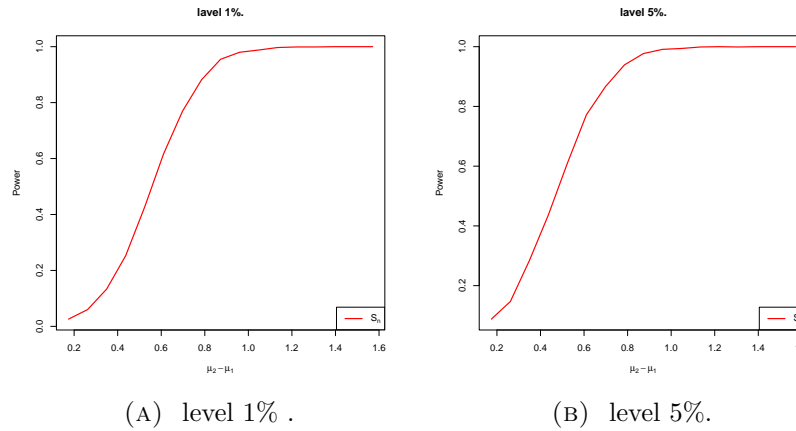


FIGURE 12. Plot of the power functions the CVMC test statistic,  $S_n$  for sample of size  $n = 500$  from wrapped-Cauchy distribution with the concentration parameter  $\rho = 0.6$ , and equispaced mean differences in  $\frac{\pi}{18} \leq (\mu_2 - \mu_1) \leq \frac{\pi}{2}$ , with the true changepoint at  $k^* = \frac{n}{2}$  under  $H_{1m}$ .

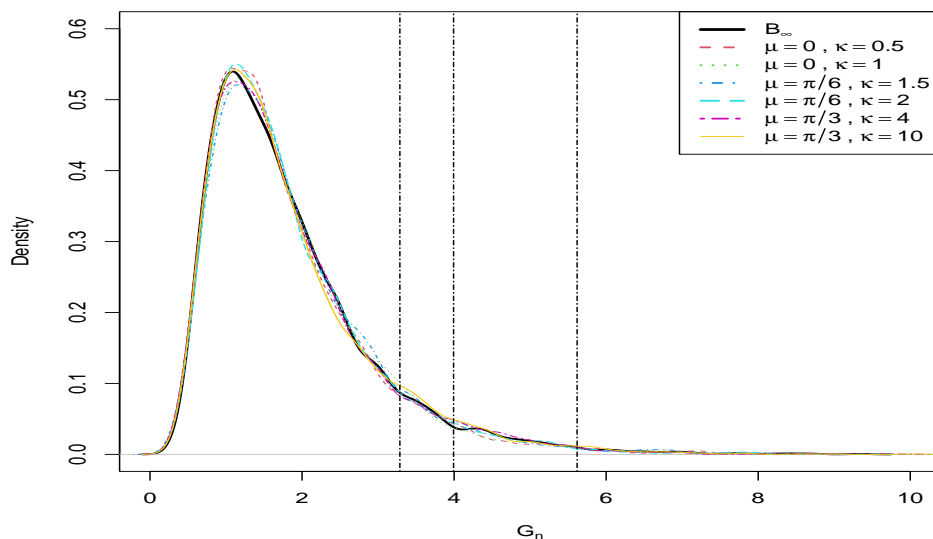


FIGURE 13. Density plot of the test statistic,  $\mathcal{G}_n$  under  $H_{0g}$  with a sample of size  $n = 1000$  from von Mises distribution with the different mean directions, and different concentration parameters along with density plot of the limiting random variable  $B_\infty$ , and its 0.90th, 0.95th, and 0.99th quantiles.

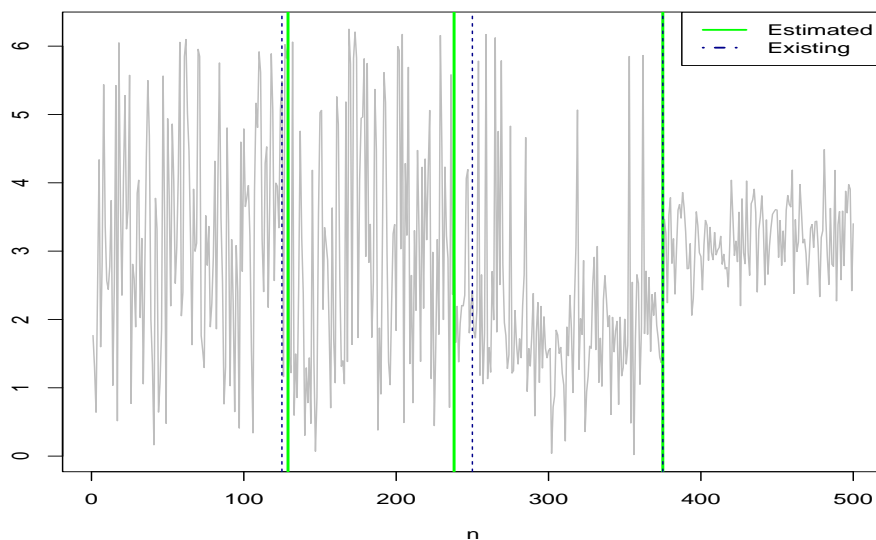


FIGURE 14. Binary segmentation for changepoint detection in either or both the parameters of von Mises distribution. Existing change points are at 125 ( $\mu = \pi$  to  $\mu = \pi/2$ ), 250 ( $\kappa = 0.5$  to  $\kappa = 2$ ), and 375 ( $\mu = \pi/2, \kappa = 2$  to  $\mu = \pi, \kappa = 4$ ). Estimated change points are at 129, 238, and 375.



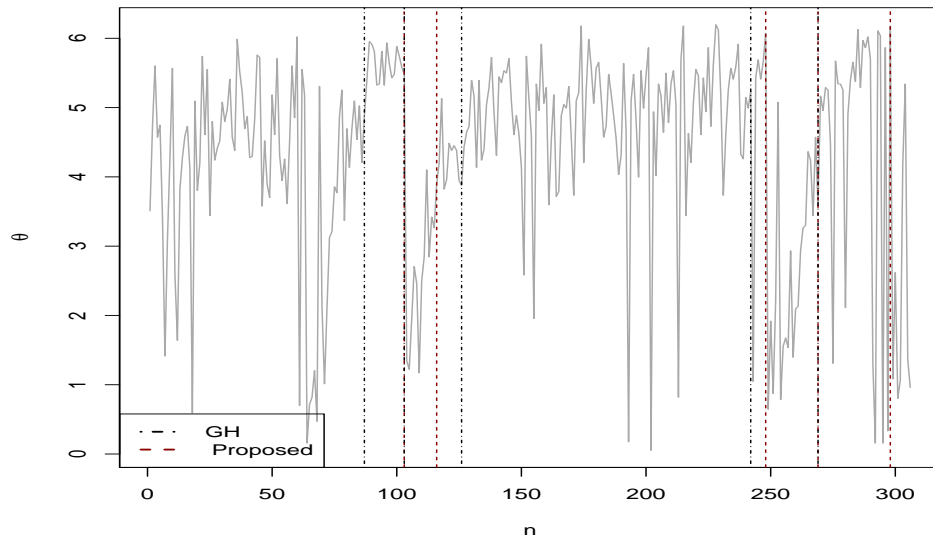


FIGURE 15. The plot of the Acrophase data with the estimated location of the changepoints in concentration, shown with the vertical lines, by the proposed method of SACC test and that of [Grabovsky and Horváth \(2001\)](#) denoted by GH.

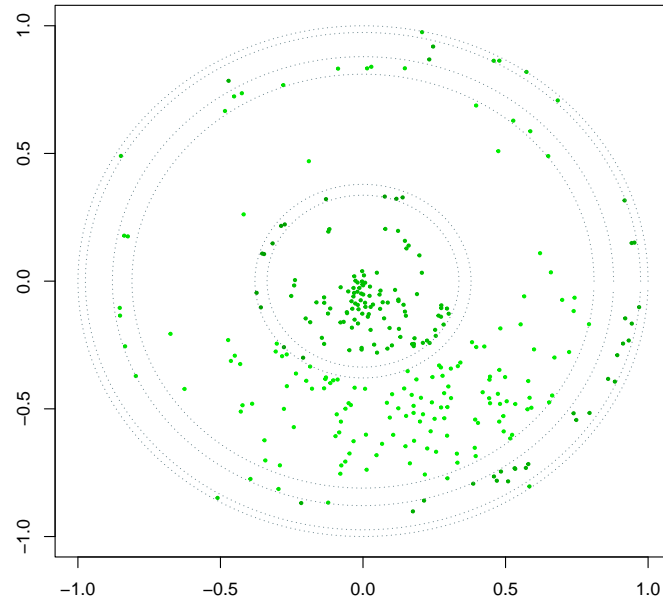


FIGURE 16. Scatter plot of the Acrophase data set. Six annular circles from the center to outward represent the corresponding estimated changepoints in the concentration parameter by the proposed method of the SACC test. The color intensity scale from lower to higher has been used to depict the concentration of angular data.

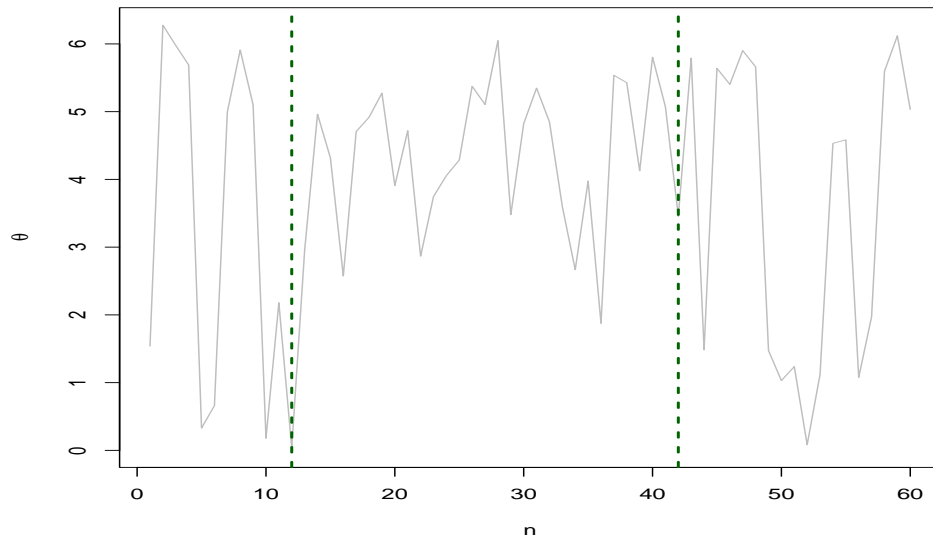


FIGURE 17. The plot of the Flare data with the estimated location of the changepoints in the mean direction, shown with the vertical lines, by the proposed method of the CVMC test.

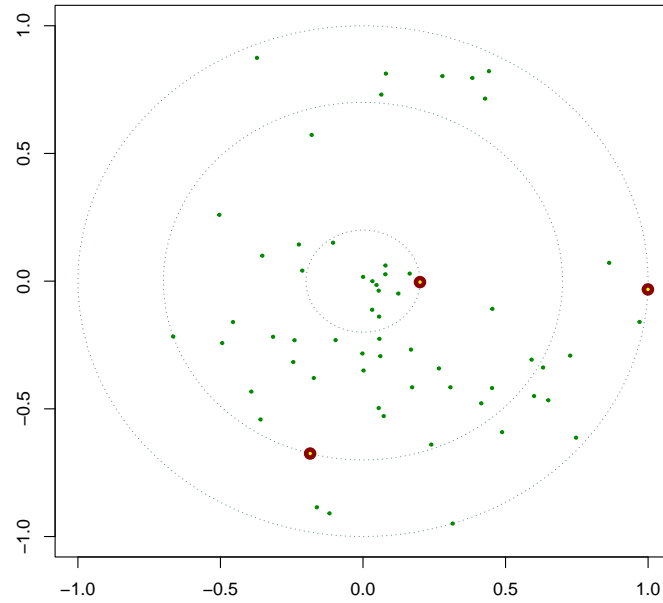


FIGURE 18. Scatter plot of the flare data set. Two annular circles from the center to the outward represent the corresponding estimated changepoints in the mean direction by the proposed method of the CVMC test. The segment-wise estimated mean is represented by red bubble plot at the outer end corresponding segment.

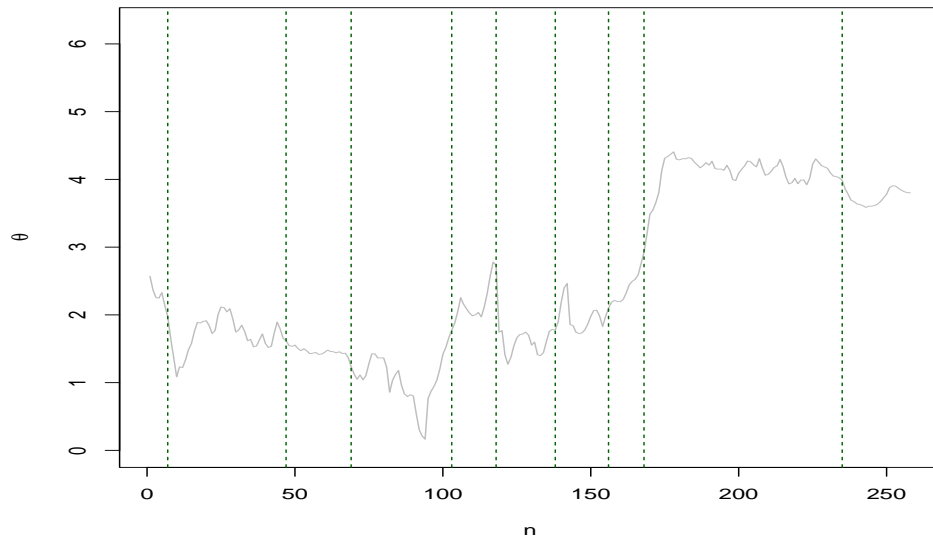


FIGURE 19. The plot of the Super Cyclonic Storm (SuCS) “AMPHAN” data with the estimated location of the changepoints, shown with the vertical lines, by the proposed method of the SAGC test.

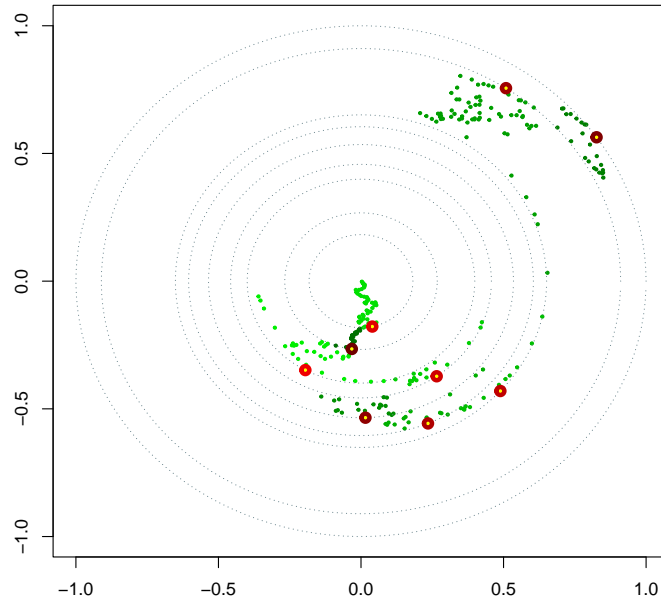


FIGURE 20. Scatter plot of the data set of the Super Cyclonic Storm (SuCS) “AMPHAN”. Eight annular circles from the center to outward represent the corresponding estimated changepoints in the mean direction and/or concentration by the proposed method of the SAGC test. The segment-wise estimated mean is represented by red bubble plot at the outer end of the corresponding segment. The color intensity scale from lower to higher is proportionate to the concentration of angular data.